NTNU – Trondheim
Norwegian University of
Science and Technology

Numerical Modelling of Brittle Failure in Ice Structures

Hanna Aarnes Nisja

Civil and Environmental Engineering (2 year)
Submission date: June 2014
Supervisor: Arne Aalberg, KT
Co-supervisor: Knut Vilhelm Høyland, BAT
Torodd Skjerve Nord, BAT

Norwegian University of Science and Technology
Department of Structural Engineering

Department of Structural Engineering
Faculty of Engineering Science and Technology
NTNU- Norwegian Univeristy of Science and Technology

ACCESSIBILITY

Open

MASTER'S THESIS 2014

SUBJECT AREA:	DATE:	NO OF PAGES:
Computational mechanics	June 10, 2014	102

TITLE:

Numerical Modelling of Brittle Failure in Ice Structures

BY:

Hanna Aarnes Nisja

SUMMARY:

The main purpose of this Master's thesis is to use finite element method to investigate if brittle failure in sea ice can be described in a force-displacement history. Four implemented material models in LS-Dyna are taken into account. This in order to study the behaviour by an interaction between drifting sea ice and offshore structures. The force-displacement curve give a sawtooth pattern by brittle failure.

Four material models were studied, characterised and used in three different numerical models. The material models are referred as *063_Mat_Crushable_Foam*, *096_Mat_Brittle_Damage*, *111_Mat_Johnson_Holmquist_Concrete* and *153_-Mat_Damage_3* in the keyword user's manual for LS-Dyna. The numerical results were compared with each other and with measured values from real experiments. The comparisons were performed with a vertical force-displacement history. All material models had results in the right order of magnitude.

From the results, it can be concluded that it seems possible to find an existing material model that can give sufficient results for interaction between ice and structures. It will be preferable to use material models with an included damage constant.

RESPONSIBLE TEACHER: Associate Professor Arne Aalberg

SUPERVISOR(S): Torodd S. Nord and Knut V. Høyland

CARRIED OUT AT: Department of Structural Engineering, NTNU

Institutt for konstruksjonsteknikk
Fakultet for ingeniørvitenskap og teknologi
NTNU- Norges teknisk- naturvitenskapelige universitet

TILGJENGELIGHET

Åpen

MASTEROPPGAVE 2014

FAGOMRÅDE:	DATO:	ANTALL SIDER:
Beregningsmekanikk	10.juni 2014	102

TITTEL:

Numerisk modellering av sprøbrudd i is

UTFØRT AV:

Hanna Aarnes Nisja

SAMMENDRAG:
I denne masteroppgaven er det benyttet numeriske analyser for å undersøke om sprøbrudd i sjøis kan beskrives i et kraft-forskyvnings-forløp. Det er sett nærmere på fire implementerte materialmodeller i LS-Dyna. Dette for å studere oppførselen som opptrer ved en interaksjon mellom sjøis og offshore-konstruksjoner. Ved sprøbrudd viser kraft-forskyvnings-kurven et sagformet kraftforløp.

Fire materialmodeller ble vurdert, karakterisert og benyttet i tre numeriske modeller. I brukermanualen til LS-Dyna er materialmodellene henvist til *063_Mat_Crushable_Foam*, *096_Mat_Brittle_Damage*, *111_Mat_Johnson_Holmquist_Concrete* og *153_Mat_Damage_3*. Materialmodellene ble sammenlignet opp mot hverandre og med måleverdier fra virkelige eksperimenter. Alle presenterte numeriske resultater hadde rett størrelsesorden sammenlignet med eksperimentene.

Fra resultatene kan det konkluderes med at det er mulig å finne en eksisterende materialmodell som kan gi gode resultater for interaksjon mellom is og konstruksjoner. Med mer forskning på området, kan den sprø oppførselen i sjøis bli gjenskapt. Det er foretrukket å bruke materialmodeller med en inkludert skadekonstant.

FAGLÆRER:	Førsteamanuensis Arne Aalberg
VEILEDER(E):	Torodd S. Nord og Knut V. Høyland
UTFØRT VED:	Institutt for konstruksjonsteknikk, NTNU

NTNU
Norges teknisk-naturvitenskapelige universitet

Fakultet for ingeniørvitenskap og teknologi

Institutt for konstruksjonsteknikk

MASTEROPPGAVE VÅREN 2014

Hanna Aarnes Nisja

Modellering av sprøbrudd i is

Numerical Modelling of Brittle Failure in Ice Structures

1. Bakgrunn/background

- Sea ice in interaction with structures may cause severe loads and vibrations, and a proper understanding of the behavior of ice is therefore necessary. In this investigation the properties and behavior of ice is studied. Several material models exist in the commercial FE programs, but there is a large need for work in the field of verification and comparison with physical experiments.

2. Gjennomføring

Oppgaven kan gjennomføres med følgende elementer:

- Redegjørelse for egenskap og oppførsel til is.
- Gjennomgang av ulike beregningsmodeller for is, og redegjørelse for tidligere undersøkelser (forsøk og datamaskinberegninger).
- Gjennomgang av FE modeller for isoppførsel.
- Simuleringer for utvalgte forsøk, sammenligning og diskusjon.

Kandidatene kan i samråd med faglærer velge å konsentrere seg om enkelte av punktene i oppgaven, eller justere disse.

3. Rapporten

Oppgaven skal skrives som en teknisk rapport i et tekstbehandlingsprogram slik at figurer, tabeller og foto får god rapportkvalitet. Rapporten skal inneholde et sammendrag, evt. en liste over figurer og tabeller, en litteraturliste og opplysninger om andre relevante referanser og kilder. Oppgaver som skrives på norsk skal også ha et sammendrag på engelsk. Oppgaven skal leveres igjennom «DAIM».
Sammendraget skal ikke ha mer enn 450 ord og være egnet for elektronisk rapportering.
Masteroppgaven skal leveres innen 10. juni 2014.

Trondheim, 14. januar 2014

Arne Aalberg
Førsteamanuensis, Faglærer

Abstract

The main purpose of this Master's thesis is to use finite element method to investigate if brittle failure in sea ice can be described in a force-displacement history. Four implemented material models in LS-Dyna are taken into account. This in order to study the behaviour by an interaction between drifting sea ice and offshore structures. The force-displacement curve give a sawtooth pattern by brittle failure.

The selected material models were determined after research of previous work for numerical modelling of ice. Material models used for similar materials, like concrete and granite were also considered. A litterature review was conducted to understand the properties of S2 sea ice, and its behaviour under compression.

Four material models were studied, characterised and used in three different numerical models. The material models are referred as *063_Mat_Crushable_Foam*, *096_Mat_Brittle_Damage*, *111_Mat_Johnson_Holmquist_Concrete* and *153_Mat_Damage_3* in the keyword user's manual for LS-Dyna.

The numerical results were compared with each other and with measured values from real experiments. The comparisons were performed with a vertical force-displacement history. All material models had results in the right order of magnitude.

From the results, it can be concluded that it seems possible to find an existing material model that can give sufficient results for interaction between ice and structures. It will be preferable to use material models with an included damage constant.

Due to recent research, there must be performed further improvements regarding the material modells and the numerical set-up. A suggestion is to SPH in LS-Dyna. The non-linear finite element code IMPETUS-Afea can be a good replacement for LS-Dyna, due to its computational efficiency.

Sammendrag

I denne masteroppgaven er det benyttet numeriske analyser for å undersøke om sprøbrudd i sjøis kan beskrives i et kraft-forskyvnings-forløp. Det er sett nærmere på fire implementerte materialmodeller i LS-Dyna. Dette for å studere oppførselen som opptrer ved en interaksjon mellom sjøis og offshore-konstruksjoner. Ved sprøbrudd viser kraft-forskyvnings-kurven et sagformet kraftforløp.

De valgte materialmodellene ble bestemt på bakgrunn av hva som tidligere er gjort av numeriske analyser for is. Det er også sett på hva som benyttes for lignende materialer, som betong og granitt. Et litteraturstudie ble gjennomført for å forstå egenskapene til is og isens oppførsel under trykk.

Fire materialmodeller ble vurdert, karakterisert og benyttet i tre numeriske modeller. I brukermanualen til LS-Dyna er materialmodellene henvist til *063_Mat_Crushable_Foam*, *096_Mat_Brittle_Damage*, *111_Mat_Johnson_Holmquist_Concrete* og *153_Mat_Damage_-3*. Materialmodellene ble sammenlignet opp mot hverandre og med måleverdier fra virkelige eksperimenter. Alle presenterte numeriske resultater hadde rett størrelsesorden sammenlignet med eksperimentene.

Fra resultatene kan det konkluderes med at det er mulig å finne en eksisterende materialmodell som kan gi gode resultater for interaksjon mellom is og konstruksjoner. Med mer forskning på området, kan den sprø oppførselen i sjøis bli gjenskapt. Det er foretrukket å bruke materialmodeller med en inkludert skadekonstant.

Siden numerisk analyse for is kun er sett på de senere årene, må ytterligere forbedringer gjennomføres for både materialmodeller og de numeriske oppsettene. Et forslag er å benytte SPH i LS-Dyna. Den ikke-lineære elementkodemodellen IMPETUS-Afea kan være en god erstatning for LS-Dyna, på grunn av kortere beregningstid.

Preface

This Master's thesis has been written as the final evaluation of the master's degree in Civil and Environmental Engineering, within computational mechanics, at Norwegian University of Science and Technology (NTNU). The amount of work is equal to 30 credits.

The main purpose of the thesis is to investigate if implemented material models in LS-Dyna can be used to recreate ice actions towards an offshore structure. Four material model are taken into account. The thesis include description of related aspects of ice mechanics, theory and characterisation of the four material models and simulation of numerical models that are further compared with existing results. The simulations are carried out in the explicit non-linear program LS-Dyna V971 R7.

I would like to thank my supervisor Arne Aalberg and co-supervisors Torodd S.Nord and Knut V. Høyland for invaluable response and guidance. I would also like to thank Torodd Berstad for the considerable assistance in the numerical work.

A thank also goes to Erland M. Schulson and Ekaterina Kim regarding my questions to the behaviour of ice, and Marion Fourmeau and Hieu Nguyen Hoang for their time according my questions to the material model Holmquist-Johnson-Cook.

Finally, I would like to thank my friends and family for their support.

Trondheim, June 10, 2014

Hanna Aarnes Nisja

Contents

List of Tables

List of Figures

Chapter 1

Introduction

Due to increased human activity in Arctic regions, interaction between ice and offshore structures will occur more frequently. The problems are among others, huge ice floes drifting from onshore and drifting first-year or multi-year sea ice. During interaction, ice failure can occur in a ductile and brittle manner. The brittle ice failure is important to understand in order to design structures in ice-choked waters.

There exists a number of investigations of ice actions, from both laboratories and different locations in the Arctic regions. The purpose is to understand how the properties of sea ice affect the brittle ice failure during ice-structure interaction.

In general, experiments from laboratory and in-situ are expensive and time consuming. Therefore, it is of big interest to develop numerical simulations for the situations described above. This is the main purpose of the Master's thesis; use existing material models to investigate if they can recreate brittle failure for S2 sea ice under compression.

In recent years, an increasing amount of work regarding simulation

of ice actions using finite element models has been published. If experimental tests can be replaced with numerical simulations for some instances, it may be much more cost effective and less time consuming to design offshore structures against ice actions.

To find a material model that renders the behaviour of ice is not a trivial task. For instance, Robert E. Gagnon has simulated ice several times with a material model initially intended for crushable foams. The situations were, i.a., ice crushing of a pyramid shaped model and collision between a loaded tanker and a bergy bit. More about the models is given in the papers by Gagnon (2011) and Gagnon and Wang (2012), respectively. von Bock und Polach and Ehlers (2013) presented a numerical analysis for model-scaled ice using a damage material model by Lemaitre, where air and water voids were taken into account.

The material models stated above, are implemented in the explicit non-linear 3D FEA program LS-Dyna. LS-Dyna contains a suite of several material models, and is used for all analyses in the thesis. The material model for crushable foams and the damage model by Lemaitre, are used in the presented numerical simulations.

To determine the material models, it is looked at previous use for ice and similar brittle materials, like concrete and granite. The selected material models are referred to in the keyword user's manual of LS-Dyna as *063_Mat_Crushable_Foam*, *096_Mat_Brittle_Damage*, *111_Mat_Johnson_Holmquist_Concrete* and *153_Mat_Damage_3*. In this thesis they are announced as Crushable Foam, Brittle Damage, Holmquist-Johnson-Cook (HJC) and Lemaitre Damage model, respectively.

The material models are used in three numerical models, which are presented in the numerical part of the thesis. The main numerical model is based on an experimental measurement of ice from Schulson's laboratory, conducted by Kim et al. (2012). The experiment involves an interaction between a spherically-shaped indenter and a

freshwater ice specimen.

The ice specimen is confined with four plates, towards movement in the horizontal direction. By confinement, a triaxial loading occurs. This is a good resemblance to what takes place in the nature, where a small piece of a larger ice floe surrounds the piece. The two other simulations are a single volume element and a drifting ice sheet towards an offshore structure developed by Hilding et al. (2012).

There are made assumptions regarding to the numerical simulations. The ice action is normal to the loading plane, and by failure the elements will erode. The extrusion of ice is therefore neglected, due to element erosion. Development of cracks, i.e. shear band, is also ignored. Kari Kolari works with a damage model, which should describe the physical aspect of wing cracks.

Experimental measurements on ice by Erland M. Schulson is the main source according to the parameter study. Several of his papers and the book about creep and fracture of ice by Schulson and Duval (2009) are widely used. The paper by Timco and Weeks (2010) is also applied, where it is looked at the stage of knowledge and applications of the engineering properties of sea ice. Løset et al. (2006) describe actions performed by ice on arctic offshore and coastal structures.

As mentioned, the scope of this thesis is to use existing numerical models from LS-Dyna to recreate brittle ice crushing failure towards an offshore structure. The ice alone, is first-year S2 sea ice with a temperature at -10°C. In the next section, the outline of this thesis is given.

1.1 Thesis Outline

The theoretical background in Chapter 2, gives the necessary physical and mechanical properties of sea ice. Further, it includes a description of ductile and brittle behavior, interaction between sea ice and structures, and continuum mechanics with damage and fracture mechanics. The theory of each material model is given in the last section of the chapter.

Chapter 3 is the part where the numerical models are described, together with the characterisation of the parameters in the material models. It will contain a description of how the material parameters are determined.

The results are presented in Chapter 4, and further discussed in Chapter 5. Chapter 6 and Chapter 7 includes the conclusion and further work, respectively.

Chapter 2

Theoretical background

Sea ice is a complex material that is composed of solid ice, brine and gas. Its properties depend on the size and orientation of the crystals, temperature, salinity, density, impurity etc. (Løset et al., 2006).

The properties of sea ice are highly variable depending upon the material's environmental history, which could mean that the ice can change along the kilometers of continuous ice sheet. This will cause different physical and mechanical properties. The physical properties are, for instance, microstructure, thickness, salinity, porosity and density. While the mechanical properties include tensile, flexural, shear, uniaxial compression and multiaxial compression strength, failure envelope, creep, Young's modulus, Poisson's ratio, fracture toughness and friction.

Due to the dependency of physical and mechanical properties, the two next sections deal with the properties of first-year sea ice that is applicable for later use in the thesis. Further the ductile and brittle behaviour of ice will be presented, as well as the damage and fracture mechanics. At the end of this chapter there is an introduction of the four material models that are further used in the numerical analyses.

2.1 Physical Properties of Sea Ice

2.1.1 The Structure of S2 Sea Ice

To define the properties of ice, Michel and Ramseier (1969) came up with a classification system that deals with the texture of different types of ice. Most of the ice over the continental shelves of the Arctic Ocean is S2 sea ice, according to the classification system.

By definition, S2 ice has a vertical columnar crystal structure with a randomly oriented c-axis in the horizontal direction. In Figure 2.2 the c-axis is oriented in the X_1-X_2 plane.

As just mentioned, the two illustrations below show S2 sea ice and S2 freshwater ice. The columnar axis is parallel to the direction of heat flow, axis defined as X_3. Sea ice and freshwater ice have the same microstructure and grow in a similar manner. However, there is a significant difference.

Sea ice is weaker than freshwater ice, because of entrapped small droplets of high saline water called brines. Sea ice also forms and expels salt into the underlying ocean water, through the brine drainage channels viewed in Figure 2.1. The brines in sea ice are unable to support shear stress, which causes an easier deformation compared to freshwater ice.

The first-year sea ice contains a higher brine volume than multi-year sea ice, since the brines in the multi-year ice will drain through the ice as it melts and grows.

Figure 2.1 is a schematic drawing that view several aspects of the structure to first-year sea ice, with horizontal and vertical thin sections. The fabric diagram, to the right in the figure, views the c-axis from a horizontal cross section. Note the development of string c-axis alignment in the horizontal plane in the lower part of the diagrams, i.e. the major layer is a typically S2 ice.

Above the columnar ice there is a granular layer, which has a randomly oriented c-axis (also viewed in the fabric diagram). The most noticeable change in the upper part of the columnar zone is the significant increase in grain size with depth, due to the growth period (Weeks and Assur, 1967).

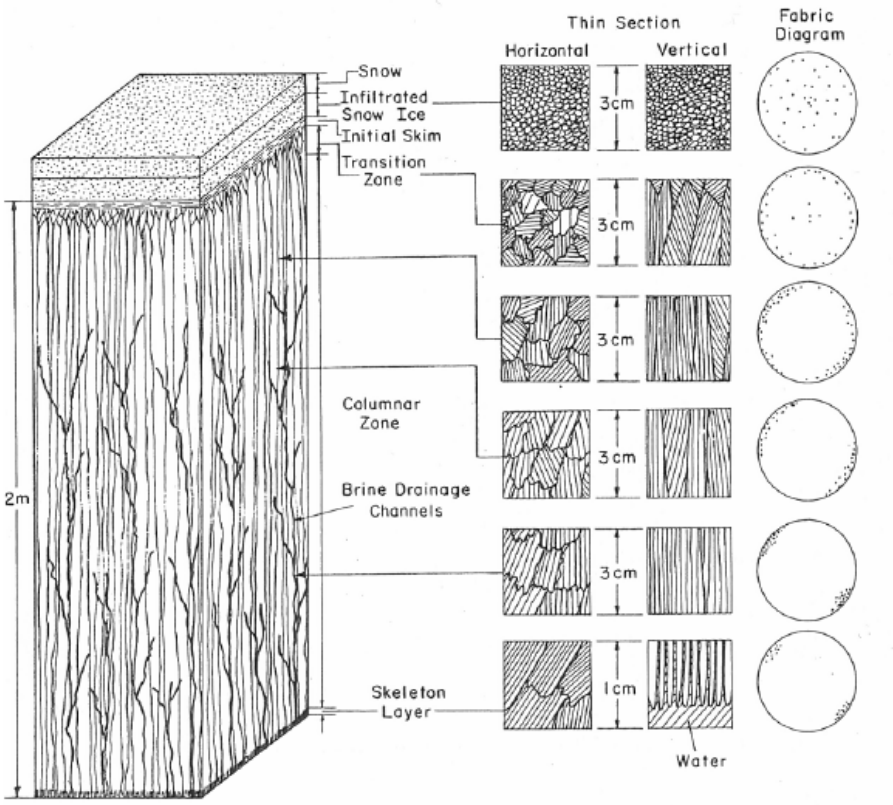

Figure 2.1: Structure of first-year sea ice above water level. (Løset et al., 2006)

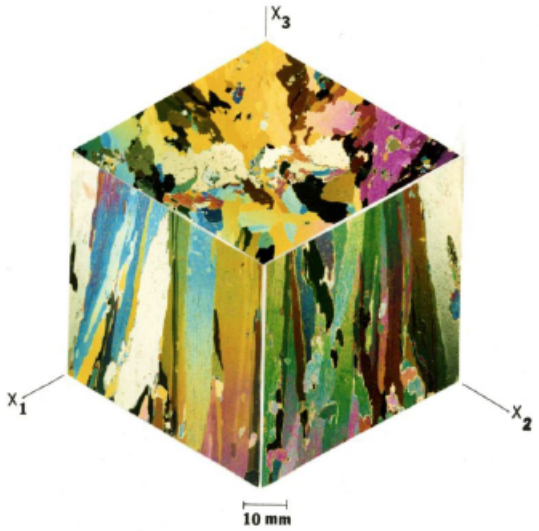

(a) Sea ice

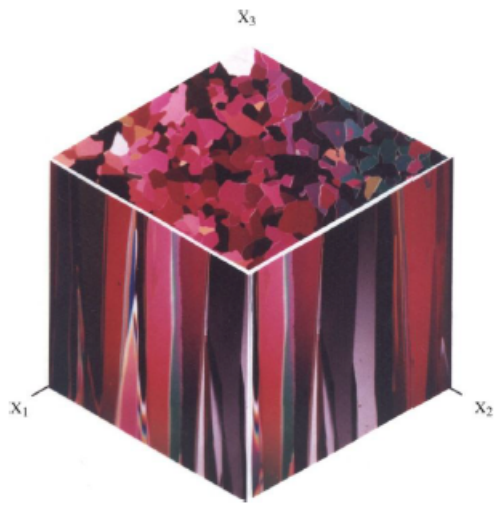

(b) Freshwater ice

Figure 2.2: Composite photographs of thin sections viewed through cross-polarizing filters showing the X_i coordinate system and the macroscopic structure of (a) S2 sea ice and (b) S2 freshwater ice. (Schulson, 2010)

Granular ice and columnar S2 ice are isotropic and transversely isotropic (orthotropic), respectively. The S2 ice is isotropic in the X_1-X_2 plane, which is an advantage when material parameters of the S2 sea ice should be determined. Further first-year S2 sea ice will be considered, and announced as S2 sea ice.

When characterising ice, it is important that the test data is measured under similar conditions. Therefore, several parameters are found from experiments performed in Erland M.Schulson's laboratory. Information is found from many of his papers, the book "Creep and Fracture of Ice" by Schulson and Duval (2009) and a personal conversation (Schulson, 2014)

2.1.2 Density

Knowledge of the density of sea ice is important in many applications. Measurements which represent the in situ density of first-year sea ice range from 840 kgm^{-1} to 910 kgm^{-1} for the ice above the waterline, and 900 to 940 kgm^{-1} for the ice below the waterline (Timco and Weeks, 2010). Gratz and Schulson (1997) studied columnar saline ice under triaxial loading, and they calculated the average density to be 910$\pm$3 kgm^{-1}.

2.2 Mechanical Properties of Ice

In the preamble several mechanical properties are mentioned. In this section, relevant topics for further study are included; compressive, tensile and shear strength, Young's modulus and Poisson's ratio. The fracture toughness, together with fracture mechanics, is described in Section 2.5.2.

2.2.1 Compressive Strength

The compressive strength is a fundamental property of sea ice. Observations of both large and small-scale sea ice under loading show that ice often fails in compression.

Under a multi-axial state of stress, it is most common that compressive failure occurs (Schulson and Duval, 2009). The reason is that materials within the compressive zone are constrained by the other surrounding materials. Therefore, a confinement induces that a bi-axial and triaxial stress state have large effect on the strength and mode of failure.

Schulson and Gratz (1999) did experimets for three regimes of a Coulombic[1]-like behaviour, where the current is in the third regime.

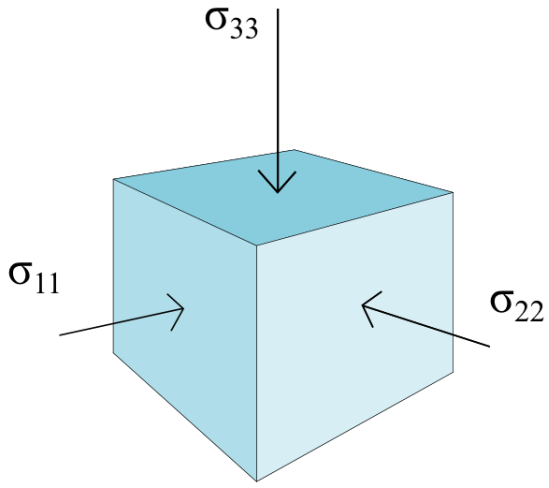

Figure 2.3: Stress distribution in the third regime, $\sigma_{33} >> \sigma_{11} = \sigma_{22}$.

[1]Coulombic faulting occurs under brittle regime, and at low confinement

The third regime is defined as; when the ice is loaded mainly along the columns, confinement across the columns increase along column stress at failure, i.e. $\sigma_{33} >> \sigma_{11} = \sigma_{22}$ (Figure 2.3).

Figure 2.4 is a graphical view of the measurements by Gratz and Schulson (1997), where $\sigma_{33,f}$ is plotted against $\sigma_{22,f}$ and $\sigma_{11,f} = \sigma_{22,f}$. The S2 sea ice is in the third regime, described above. The figure shows a linear increase between the vertical and the horizontal stresses, see Figure 2.3 for description of the directions.

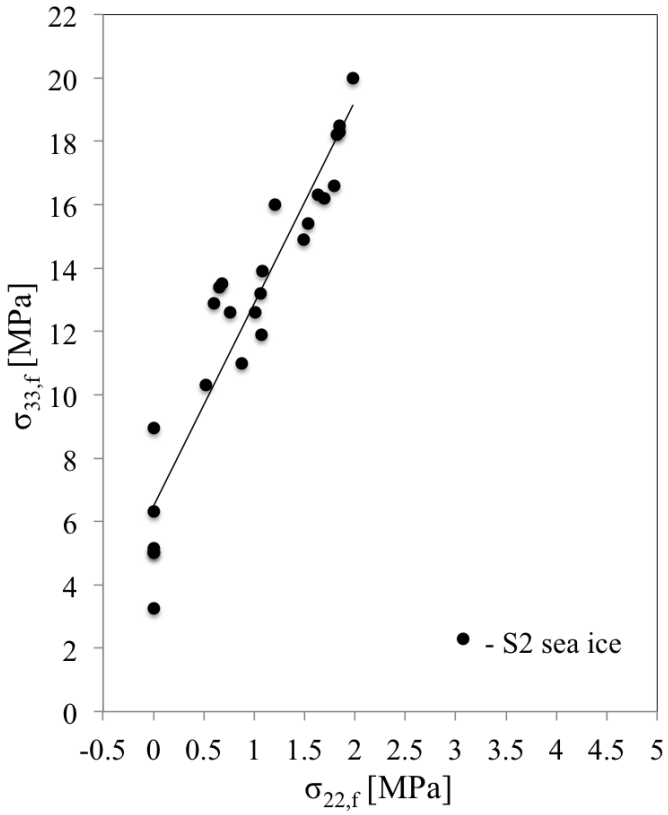

Figure 2.4: Compressive strength of S2 sea ice in the third regime at -10°C, $\sigma_{11,f} = \sigma_{22,f}$. Data from Gratz and Schulson (1997)

From the measured data of uniaxial strength by Jones (1997), the values are in the order of 8 MPa to 12 MPa. Schulson and Duval (2009) renders a graph for unconfined uniaxially compressive strength versus strain, which gives a range from approximatly 0.12 MPa to 20 MPa. The basal plane was inclined by 45° to the direction of loading. It should be noted that, the S2 ice is weakest at 45° compared to 0° and 90°.

2.2.2 Tensile Strength

The tensile strength defines the maximum tensile stress that ice can sustain before failure. The tensile strength is important for predicting both large-scale ice movements and local ice forecasting. (Timco and Weeks, 2010)

Results from Richter-Menge and Jones (1993), Saeki et al. (1978) and Dykins (1970) indicate a decrease in tensile strength with increase in temperature. For columnar ice, the tensile strength is about three times higher when an ice specimen is loaded with tensile stress exerted parallel to the growth direction, i.e. vertically loaded (Timco and Weeks, 2010).

Figure 2.5 gives the tensile strength of S2 sea ice loaded uniaxially across the columns versus temperature, at strain rate of $10^{-3}s^{-1}$. The tensile strength is dependent on the temperature; as the temperature increase, the tensile strength decrease. From figure 2.5, the measured tensile strength range is 0.63±0.12 MPa at -10°C.

2.2.3 Shear Strength

There is considerable scatter in the measured shear strength of sea ice. A lot of the test results are generated using test techniques which impose unrealistic normal stress in the failure plane (Timco and Weeks,

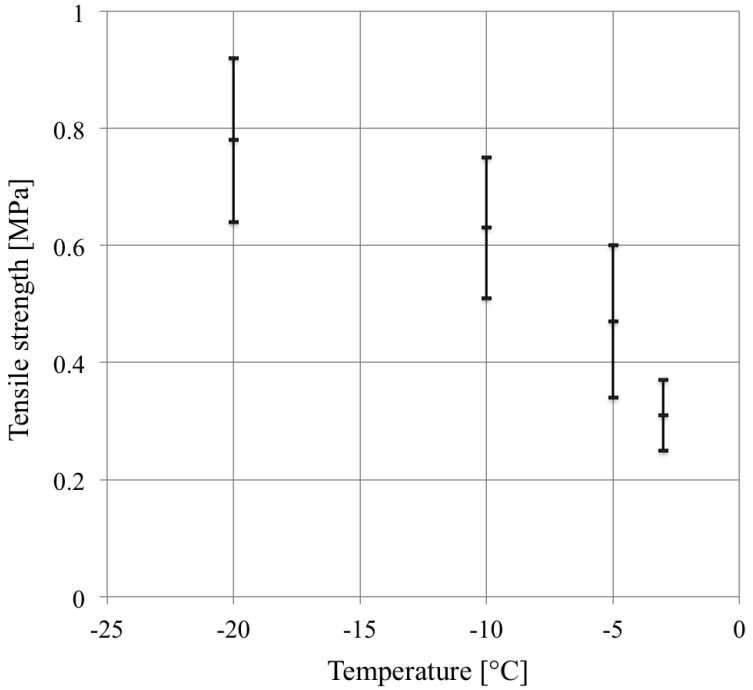

Figure 2.5: Tensile strength of columnar first-year S2 ice, at strain rate of $10^{-3}\ s^{-1}$. Data from Richter-Menge and Jones (1993)

2010). According to Timco and Weeks (2010) shear strength values from the more reliable tests ranged from 550 kPa to 900 kPa for columnar sea ice.

2.2.4 Young's Modulus and Poisson's Ratio

The Young's modulus and Poisson's ratio are two important values in ice mechanics, since the effects of the sea ice viscoelasticity is significance.

The Young's modulus E is defined as the ratio of the stress σ to the

strain ε during elastic behaviour. The relationship is described by Hooke's law, $\sigma = E\varepsilon$. Note that in ice mechanics, the term Young's (elastic) modulus is not entirely correct, because of the viscoelastic strain in Equation 2.1. Young's modulus is often expressed as effective modulus or the strain modulus. In this thesis the term Young's modulus will be used, since it is common practice in the keyword user's manual in LS-Dyna.

$$\varepsilon^t = \varepsilon^e + \varepsilon^{ve} + \varepsilon^{vp} \tag{2.1}$$

In Equation 2.1, ε^e is the instanteneous elastic strain, ε^{ve} is the viscoelastic strain (delayed elastic) and ε^{vp} is the viscoplastic strain.

There is a significant increase in the value of E with decreasing temperature and decreasing brine volume (Timco and Weeks, 2010), see Equation 2.2 where v_b is the brine volume. The value of Young's modulus at low brine volumes are characteristically in the range of 9 to 10 GPa.

$$E = 10 - 0.0351 v_b \tag{2.2}$$

According to Schulson and Duval (2009) the most accurate values for Young's modulus to date has been obtained by Gammon et al. (1983). The samples was characterised as first-year columnar sea ice, sampled at -3°C and tested at -16°C. Five values for the modulus were determined, due to the Ih[2] ice. The values ranged from 3.1 GPa to 14.3 GPa, depending on the orientation of the axes. An average value of Young's modulus for isotropic ice was determined to 9.3 GPa.

The isotropic average value for Poisson's ratio was determined to 0.325 by Gammon et al. (1983). In the paper by Timco and Weeks (2010) the value for sea ice is determined with a mean value of

[2]Ih is hexagonal crystal form of ordinary ice

0.295±0.009. A Poisson ratio of 0.33 is suggested for sea ice according to the same paper.

By Equation 2.3 the shear modulus G can be obtained by the Young's modulus E and Poisson's ratio ν. The shear modulus is thirty-eight percent of the value of E and it varies in a similar manner with the "state" of the sea ice.

$$G = \frac{E}{2(1+\nu)} \tag{2.3}$$

Another modulus which is dependent on Young's modulus and the Poisson's ratio, is the bulk modulus. This is useful for the characterisation in Holmquist-Johnson-Cook material model.

$$K = \frac{E}{3(1+2\nu)} \tag{2.4}$$

2.3 Brittle and Ductile Behaviour under Compression

Ice exhibits two kinds of inelastic behaviour under compression. Under high rates of deformation the material is brittle, and it is ductile under lower rates of deformation (Schulson, 2001).

Figure 2.7 gives a selection of results from the laboratory test by Kim et al. (2012). One of the numerical models are based on the experiment. The test set-up is shown in Figure 2.6, and further described into detail in Section 3.2.

The confined ice specimen is loaded with a spherically-shaped indenter. With a vertical velocity at 5.08 mm/s for test number EK7 and EK8, the behaviour is in the brittle dominate regime. The results

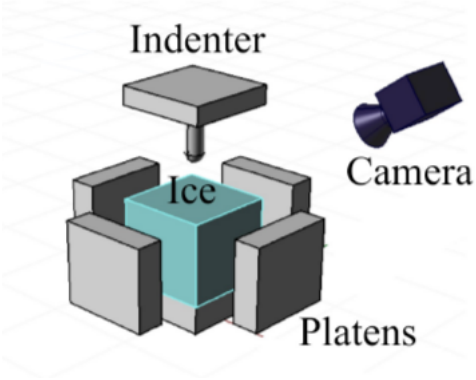

Figure 2.6: Laboratory test set-up with a confined ice specimen and an indenter, conducted by Kim et al. (2012).

from test number EK14 with a indenter velocity a tenth less than the others, shows a ductile behaviour.

The test measurements show that by a ductile dominate regime, the loads reach higher levels than for a brittle. Also note that by higher velocities, the ice specimen got a brittle failure.

The interaction between structural deformation and an advancing ice sheet produces alternating creep and brittle crushing in the same event. Which esulting in a saw tooth formed action, as seen in Figure 2.7.

When the ice sheet fails at a certain loading level, the stored energy in the structure is released to move the structure back to its original position. This results in a high relative speed with respect to the ice, which causes brittle failure. This type of interaction often produces either transient or steady-state vibrations, which is not considered further (Løset et al., 2006).

Figure 2.8 is a schematic view of the stress-strain curves for polycrystalline ice under compression as a function of strain rate that shows the transition, $\dot{\varepsilon}_t$, between ductile and brittle behaviour.

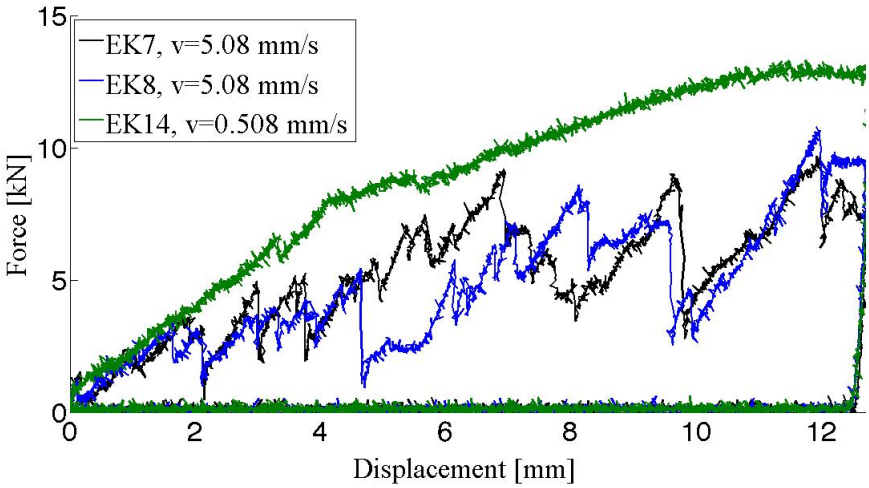

Figure 2.7: Force-displacement history for ductile and brittle behaviour from laboratory measurements. Data from Kim et al. (2012).

The ductile behaviour, left hand side of the figure, have a smooth stress-strain curve that rises and then either levels off or reaches a maximum followed by descent towards a plateau. In comparison, brittle behaviour is characterised by a stress-strain curve that rises pseudo linearly and then suddenly drops off after a strain of approximately <0.003, with little evidence of roll-over. The sudden failure for brittle behaviour is marked in the load curve with a cross. (Schulson and Duval, 2009).

The strain rate $\dot{\varepsilon}_t$ is around one to four orders of magnitude greater in compression than under tension. The reason for the higher transition strain rate is that brittle compressive strength is considerably greater than the tensile strength (Schulson and Duval, 2009), i.e. ice is stronger in compression than tension.

From Figure 2.8, there is illustrated that by increasing strain rate the ductile "peak" stress will increase. Since the maximum ductile behaviour also increase with lower temperatures, it can be stated that

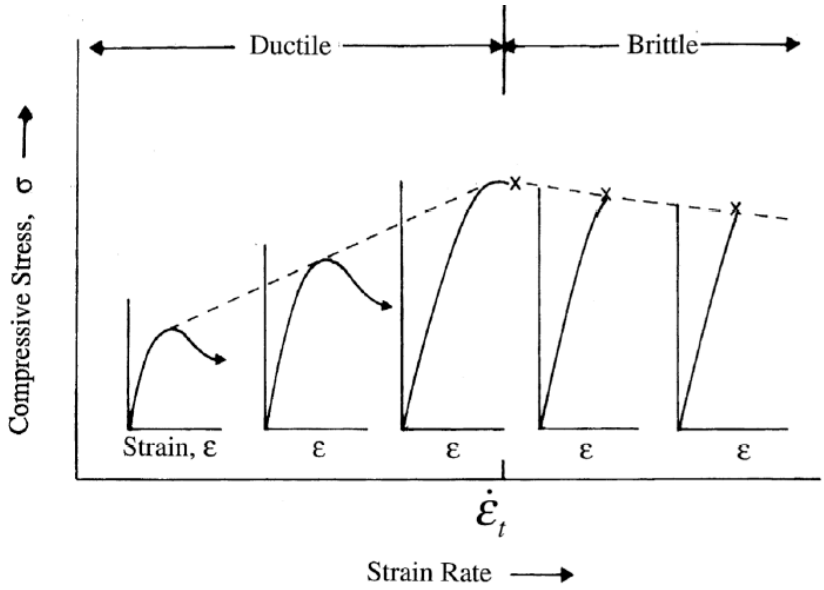

Figure 2.8: Schematic of stress-strain curves for polycrystalline ice under compression as a function of strain rate. At low rates of compression ice exhibits ductile behaviour. At high rates of compression ice exhibits brittle behaviour. (Schulson and Duval, 2009).

ice is stronger by high strain rates and low temperatures. Gradually, the ice will exhibit brittle behaviour, and after failure the strength decreases (Schulson, 2001).

Ice can exhibit Coulombic (C) faulting and plastic (P) faulting within brittle and ductile regime, respectively. The C-faulting develops under lower degree of triaxial confinement, while P-faulting develops under higher triaxial confinements. Coulombic faulting is a frictional based process.

The triaxial strength of both S2 sea ice and freshwater ice exhibits three regimes of behaviour. One of them is loading mainly along the columns. Which is called the third regime, and is already presented in Section 2.2.1.

In the third regime the compressive strength increase linearly in proportion to the lower of the two across-column confining stresses, illustrated in Figure 2.3. Correspondingly failure occurs through C-faulting. C-faulting is characterised by macroscopic faults, comprised of a narrow band of microcracks, oriented around 30 degrees from the direction of maximum shortening by -10°C. More about the Coulomb failure can be read in the book of Schulson and Duval (2009).

2.4 Interaction of Ice-Structure

As stated in Section 2.3, the brittle failure is important in structure design by interaction between ice and structures. Indentation of ice can occur, for instance, when floating ice meets a bridge pier, a lighthouse or an offhore platform. If the interaction force is too high, the structure will fail. The book of Løset et al. (2006) is a good source on ice actions on arctic structures, and this chapter is mainly dependent on the book.

The forces generated during ice floe impact against a structure depend on the mass and the initial velocity of the ice. Interaction between drifting ice and structures may cause formation of local and global actions, structure vibrations, abrasion of structure's surface etc.

A local action acts on a relatively small part of the contact area where the ice meets the structure. The global action F_G exerted the whole structure, and can be determined as the integral of the projections of local actions p_l acting simultaneously over the contact surface,

$$F_G = \int\int p_l \, dA \tag{2.5}$$

where A is the real contact surface between ice and structure, which means the effective contact area at the same instant of time. It follows

from this equation that the contact area and pressure intensity is dependent on the global load. For instance, a low pressure over a wide area can be worse than high local pressure in a narrow area. In Figure 2.9 a interaction between ice and a structure is illustrated.

Different failure modes in the ice can occur when it interacts with a structure, i.e. creep, radial and circumferential cracking, buckling, spalling and crushing. Løset et al. (2006) and Schulson and Duval (2009) have litterature on these subjects, while Sodhi and Haehnel (2003) describe the crushing failure mode during edge indentation of moving ice floes, like creep and brittle failure.

Figure 2.9 illustrates a three step interaction between ice and a structure. The first figure, 2.9a, shows the development of the microcracks, then crushed ice spalls, before it disappears, from the top and bottom of a ice floe (Figure 2.9b). In the third step, Figure 2.9c, the contact area can be small. This ice will also go to failure and spall away.

When there is no contact between the ice and the structure, a gap takes place. This may cause critical actions when the interaction between the ice and the structure starts over again.

Schulson and Duval (2009) describe the behaviour like this; the load rises in a pseudo-linear manner until it reaches a sharp maximum after which it drops suddenly and becomes jerky as indentation continuous. The peak in ice stress may not coincide with the peak in ice velocity.

The most widespread scenario by an interaction between ice and structure, is the limit stress. It controls the maximum action in most cases, and corresponds to the situation when stress (compressive, shear, tensile, flexure and buckling) reaches some limit value. It is known that the ice can not endure the action that exceeds its bearing capacity (e.g. strength) (Løset et al., 2006).

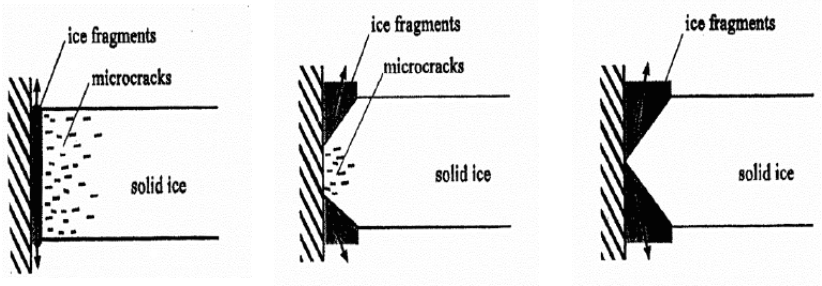

(a) Microcracking (b) Intermediate (c) Flaking

Figure 2.9: Fragmentation of drifting ice towards an offshore structure. (Saeki and Ozaki, 1980)

2.5 Continuum Mechanics

In continuum mechanics, the intention is to describe the behaviour of materials by ignoring its particulate nature. A continuum is an area that can be divided infinitely, and there is no individual particles. The simplification makes it possible to investigate the movement of a material on a scale larger than the distances between particles. In this case, the S2 sea ice is assumed as a continuum.

Løset et al. (1998) define the continuum mechanics as mechanical behaviour of materials modelled as a continuous mass. This means that the actual physical discontinuities like atoms, molecules, and crystals are not considered. In engineering, the mechanics of continuous models introduces a representative volume element (RVE) on which all properties are represented by homogenised variables (Lemaitre and Desmorat, 2010). Further, the section deals with the damage and fracture mechanics.

Løset et al. (2006) describes damage and fracture mechanics like this:

- Damage mechanics. The existence of micro cracks, holes etc. is considered as damaged material, and is treated as a reduction

in strength. The local conditions around the damaged parts are not treated.

- Fracture mechanics. Assumes the existence of one dominating crack, and concentrates on the conditions loacally around the crack tip.

2.5.1 Damage Mechanics

Continuum damage mechanics is used to predict the crack initiation in structures subjected to heavy loadings. The damage discontinuities are "small" with respect to the size of the RVE, but of course large compared to the atomic spacing (Lemaitre and Desmorat, 2010).

In ice mechanics, Kolari (2007) describes the damage mechanics concept as a loss of stiffness that can be considered to be a consequence of randomly distributed microcracks. The loss can be macroscopically measured and characterised by a single damage variable.

Depending on the type of damage, scalar D, vector $\mathbf{D}$ or tensor (D_{ij} , D_{ijkl}) variables can be used. It depends on whether the material is isotropic or anisotropic.

In ice mechanics both isotropic and anisotropic material are represented. Damage in isotropic material can be defined by a scalar, or a damage tensor D_{ij} for multiaxial case. While columnar ice is anisotropic and the damage has to be represented by a fourth order tensor D_{ijkl}.

The damage scalar D represents the damage in the plane, where undamaged material by D=0 and fully damaged material by D=1. The undamaged and damaged surfaces are illustrated in Figure 2.10.

The undamaged and damaged surfaces are important to the definition of the scalar damage variable. The stress for the undamaged surface A_0 is given by $\sigma_0 = F/A_0$. The damaged surface A have to include

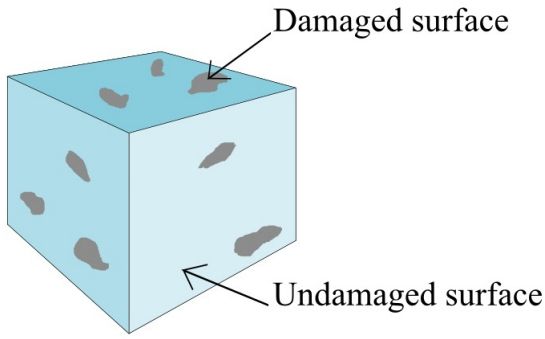

Figure 2.10: Undamaged and damaged surfaces in a material.

the a damage variable, in this case D. The effective stress acting on the resisting area can be given as,

$$\tilde{\sigma} = \frac{F}{A_0(1-D)} = \frac{\sigma}{1-D} \tag{2.6}$$

where F is the applied load.

In numerical analyses it is most common to use a damage scalar D, but there is also some material models that include the anisotropic effect. In this context, the scalar for isotropic materials is of interest.

2.5.2 Fracture Mechanics

When ice is loaded, micro cracks may appear. Once a crack is presented in a material, the question is under what conditions it will grow or propagate.

The fracture is propagation controlled when the crack is stable. While, fracture is nucleation controlled when the micro crack continues to grow after its formation, and eventually leads to failure, i.e. the

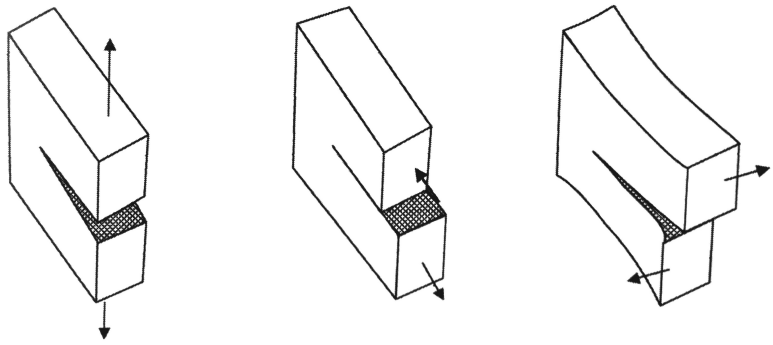

(a) mode-I (b) mode-II (c) mode-III

Figure 2.11: Three crack propagation: (a) crack opening/tensile mode; (b) crack sliding mode; (c) crack tearing mode.

crack is unstable. The nucleation controlled fracture is called brittle fracture, and is important in fracture mechanics. (Løset et al., 2006)

The principle of fracture mechanics is that energy dissipates during fast crack propagation, through ice, is governed to a large degree by the energy required to create new surfaces (Schulson and Duval, 2009). Materials with cracks will fail before an undamaged material, since the stresses around the crack tip is consideredably larger than elsewhere in the material.

Three different modes of deformation, or crack opening modes are defined in Figure 2.11. Mode-I loading refers to the opening of a crack under external load, as opposed to crack sliding mode-II or to crack tearing mode-III of the material adjacent to the crack tip. It will further be assumed that the deformation occurs in mode-I, since it is usually of greatest importance for ice.

The crack behaviour is of interest, and particularly in their resistance to propagation. This is expressed as fracture toughness K. The fracture energy per unit is crack advance given by the parameter G.

The fracture toughness in mode-I, K_I, and the toughness G define the state of a loaded crack system. When the stress intensity factor reaches a critical level of the material at hand, i.e. $K_I = K_{Ic}$ and $G = G_c$, the crack propagates. The parameters K_{Ic} and G_c are termed fracture toughness and toughness, respectively, and are given as,

$$K_{Ic}^2 = \frac{G_c E}{1 - \nu^2} \tag{2.7}$$

where E is Young's modulus and ν is Poisson's ratio. The fracture toughness depends on the loading rate and the ice type, with less variation due to temperature and grain size.

Fracture toughness is a material parameter that should be independent of the sample size. According to Schulson and Duval (2009) the parameter for sea ice ranges from around 100 kPam$^{0.5}$ for the smallest specimens (0.5m) to 250 kPam$^{0.5}$ for the largest (80m). Timco and Weeks (2010) mention that 115 kPam$^{0.5}$ is the typical value of Mode-I fracture toughness of small samples. Dempsey et al. (1999) report that the fracture toughness for the thick first-year sea ice, size-independent, is of order 250 kPam$^{0.5}$.

2.6 von Mises and Hill's Yield Criterion

Under multiaxial loading conditions, the stress can be determined by the von Mises or Hill's yield criterions for isotropic and anisotropic material, respectively. The von Mises yield criterion is one of the earliest pressure independent plasticity models, and Hill's criterion is a straightforward extension of the von Mises yield criterion.

Golding (2012) used the criterions in his Doctoral thesis to describe the effective stress of granular and columnar ice. As mentioned ear-

lier, the granular ice is isotropic and columnar ice is anisotropic (transversly isotropic) materials.

Since von Mises criterion requires less information than Hill's criterion, it will be of interest to consider both equations in a numerical simulation. Even though the Hill's criterion is most suitable for transversly isotropic materials, i.e. S2 sea ice.

von Mises yield criterion

The von Mises yield criterion is based on the assumption of isotropy and pressure insensitivity of the material, and is given in Equation 2.9.

The yield criterion is expressed by the critical yield stress σ_y^v, which is defined by the deviatoric stress tensor $J2$. The stress tensor is defined by the stresses in the principle directions σ_1, σ_2 and σ_3, see Equation 2.8.

It is assumed that the yield occurs when the second principle invariant of the stress deviator J_2 reaches a critical value k^2, i.e. $\sqrt{J_2} = k$ (Børvik and Hopperstad, 2013). The J_2 is given as,

$$J2 = \frac{1}{6}((\sigma_1 - \sigma_2)^2 + (\sigma_2 - \sigma_3)^2 + (\sigma_3 - \sigma_1)^2) \tag{2.8}$$

The effective stress σ_y^v, critical yield stress, is then further defined for granular ice,

$$\begin{aligned} \sigma_y^v &= \sqrt{3J2} \\ &= (\frac{1}{2}((\sigma_1 - \sigma_2)^2 + (\sigma_2 - \sigma_3)^2 + (\sigma_3 - \sigma_1)^2))^{0.5} \end{aligned} \tag{2.9}$$

where σ_1 is assigned to the algebraically largest value and σ_3 to the algebraically smallest value. Under uniaxial loading, $\sigma_y = \sigma_1$, since

$\sigma_2 = \sigma_3 = 0$. Several implemented material models in finite element programs are based on the von Mises yield criterion.

Hill's Yield Criterion

As described above, the von Mises yield criterion determine the effective stress for isotropic marerials. However, it is important to establish an yield criterion for anisotropic materials, because of the difference in structure. A particularly important class of anisotropy is the transversly symmetry (Børvik and Hopperstad, 2013). The Hill's criterion also describes the orientations in a material, and is given by the expression,

$$\sigma_y^H = \left\{ \frac{3[F(\sigma_{22} - \sigma_{33})^2 + G(\sigma_{33} - \sigma_{11})^2 + H(\sigma_{11} - \sigma_{22})^2]}{2(F + G + H)} \right\}^{0.5} \tag{2.10}$$

where

$$F = G = \frac{1}{2(\sigma_{u,3}^d)^2} \qquad H = \frac{1}{(\sigma_{u,1}^d)^2} - \frac{1}{2(\sigma_{u,3}^d)^2}$$

where σ_{11}, σ_{22} and σ_{33} are the three applied stresses oriented in the directions X_1, X_2 and X_3, respectively, according to Figure 2.2. The main stress σ_{11} is parallell with the c-axis of the S2 ice and σ_{33} is parallell to the column's directions.

The constants F, G and H are determined from the uniaxial failure stresses and $\sigma_{u,1}^d$ and $\sigma_{u,3}^d$ are the unconfined across-column and along-column compressive yield stresses. The unconfined across-column, 0°, and along-column, 90°, compressive yield stresses can be found from earlier measurements performed on ice specimen, where the specimen is loaded in a different direction according to the c-axis.

The proportional loading path is often given to describe the relationship between the stresses. It is possible to calculate the applied stresses from earlier measurements with the given ratios. It is expressed as (R:R_{21}:R_{31}), where R needs to be larger than one and R_{21} and R_{31} is defined as,

$$R_{21} = \frac{\sigma_{22}}{\sigma_{11}} \tag{2.11a}$$

$$R_{31} = \frac{\sigma_{33}}{\sigma_{11}} \tag{2.11b}$$

For columnar ice σ_{11} is the most compressive principal stress. σ_{22} and σ_{33} may not be the respective intermediate and minimum principal stresses (Golding, 2012).

The pressure is useful in several cases, and can be decided by applying the following equation,

$$P = \frac{\sigma_{11} + \sigma_{22} + \sigma_{33}}{3} \tag{2.12}$$

The information and equations given above is useful according to determinations of different values from earlier measurements. The proportional loading path is often given, which makes it easier to determine the material parameters to sea ice.

2.7 Material Models in LS-Dyna

In the following sections the theory regarding the four material models are taken into account. The models are further used in the numerical simulations to see if the results render the brittle behaviour by interaction between ice and structures.

In Section 3.3 the material models are characterised, while the numerical results are presented in Chapter 4. Note that the material parameters mainly have the same annotation as in LS-Dyna.

Material models for ice in numerical simulations are not well established. The challenge is to find a material model that is capable of capturing the distinctive mechanism in ice by compression.

There is of great interest to use an already implemented material model, and LS-Dyna have a large collection compared to other finite element programs. The choice of material models are based on previous use for ice and similiar materials, like concrete and granite.

In the keyword user's manual in LS-Dyna the material models are referred to as *063_Mat_Crushable_Foam*, *096_Mat_Brittle_Damage*, *111_Mat_Johnson_Holmquist_Concrete* and *153_Mat_Damage_3* (Hallquist, 2014). In this thesis they are announced as Crushable Foam, Brittle Damage Model, Holmquist-Johnson-Cook (HJC) and Lemaitre Damage Model, respectively. None of the material models are temperature dependent, and this behaviour is therefore not considered.

Gagnon has simulated ice behaviour several times with the Crushable Foam model, Gagnon and Derradji-Aouat (2006), Gagnon (2011) and Gagnon and Wang (2012). Gagnon (2011) simulated ice crushing alone, and the remaining papers contains simulation of collisions with a bergy bit.

von Bock und Polach and Ehlers (2013) used the Lemaitre Damage Model in simulation of model-scaled ice. The numerical ice model has

voids of air and water that is incorporated with a random algorithm that define 1 % of the elements as air and 4.5 % as water. The model-scaled ice has a water layer added at the top. As a simplification, components as air and water are neglected in this context.

The HJC material model is applied several times for concrete, not surprisingly since it was developed mainly for concrete. In the Doctoral thesis by Seah (2006) this model is applied to simulate penetration of granite by hard projectiles. The last material model, Brittle Damage, was chosen due to its brittle behaviour and few required parameters.

HJC and Lemaitre Damage model have an isotropic damage scalar implemented. More about damage constants in Section 2.5.1, where both isotropic and anisotropic tensors are considered. Since S2 sea ice is transversly isotropic, an isotropic damage scalar is sufficient.

In Section 2.8, a failure/erosion criterion in LS-Dyna is presented. The criterion is added to those material model that do not include a damage constant or needs to have erosion added.

2.7.1 Crushable Foam Model

The Crushable Foam model requires an input of five parameters and a loading curve; density ρ, Young's modulus E, Poisson's ratio ν, tensile stress cutoff σ_t^c, a damping coefficient and a stress-strain curve.

In the implementation of the model it is assumed that Young's modulus is constant and the stress is updated assuming elastic behaviour. Unloading is elastic to the tension cutoff stress σ_t^c, while subsequent reloading follows the unloading curve. The stress is given as,

$$\sigma_{ij}^{trial} = \sigma_{ij}^{n} + E\,\dot{\varepsilon}_{ij}^{n+0.5}\,\Delta t^{n+0.5} \tag{2.13}$$

where σ_{ij} is the stress tensor, E is the Young's modulus, $\dot{\varepsilon}_{ij}$ is the strain rate and Δt is the time increment. The magnitudes of the

principal values are then checked to see if the yield stress is exceeded. In these circumstances, the principal stress are scaled back to the yield surface σ_y,

$$\sigma_y < |\sigma_i^{trial}| \text{ then } \sigma_i^{n+1} = \sigma_y \frac{\sigma_i^{trial}}{|\sigma_i^{trial}|} \tag{2.14}$$

After the principal values are scaled, the stress tensor is transformed back into the global system; the yield surfaces for the present application.

According to Hallquist (1998) a small value for the Poisson's ratio has to be determined. The reason is to insure a flattening of the ice at the contact zone that is more reminiscent of melting rather than a flattening that induces bulking of surrounding material, such that occurs in an elastic deformation scenario with a "real" Poisson's ratio (Gagnon and Derradji-Aouat, 2006).

Gagnon and Derradji-Aouat (2006) and Gagnon (2011) used a high stress and low stress curve for the yield stress versus volumetric strain. The low stress curve represents crushed ice, while high stress is areas with undamage ice. The graphs are given in Figure 3.2.

Hallquist (2014) recommends a value between 0.05 and 0.5 for the damping coefficient. The value is useful to dampen resonant oscillation. Ice is a stiff material, and is effective damped.

2.7.2 Brittle Damage Model

The Brittle Damage model is primarly formulated for evaluating brittle damage in concrete, but it can be applied to a wide varity of brittle materials. It is particulary useful in impact simulations. The advantage for this model is that it contains a minimal set of material parameters.

The necessary parameters for the brittle damage model for ice simulation are mass density ρ, Young's modulus E, Poisson's ratio ν, tensile stress σ_t, shear stress σ_s, compressive yield stress σ_y, toughness G_c, shear retention β and viscosity η. The six first parameters are found in litterature, the others are calculated or determined by inverse modelling.

Govindjee et al. (1995) present a full description of the tensile and shear damage part of this model. Further, the general part of the model is dealt with.

Failure in the material is assumed to initiate when the first principle stress exceeds some threshold value. Three coupled surfaces are postulated to define the damage surface. There is one tensile traction and two shear tractions, that work across the smeard crack field (Govindjee et al., 1995).

The shear retention multiplied with the shear stress, $\beta\sigma_s$, represents the shear traction that is allowed across the smeard crack plane as the damage progresses, i.e. a damage rule. The shear retention indicates the percentage of elastic shear capacity that is retained after cracking. According to Govindjee et al. (1995) the shear retention factor should be determined to a small value. The shear traction σ_s' is defined as,

$$\sigma_s' \leq \sigma_s(1-\beta)(1-exp[-H_s\alpha]) \tag{2.15}$$

where the parameter H represents the softening modulus, which is chosen by the analytical program based on the element size. The shear degradation is coupled to the tensile degradation through the internal variable α, which measures the intensity of the crack field.

The fracture toughness of the material should be entered as fracture energy per unit area crack advance, i.e. the toughness. The toughness G_c is important for a stabile calculation process. It can be determined from Equation 2.7, with a dependency to the fracture toughness K_{Ic}, Young's modulus E and Poisson's ratio ν.

The viscosity of the material is also crucial on the stability of the calculation process. In order to avoid error termination, values of the viscosity between 0.71 and 0.73 MPa are recommended.

2.7.3 Holmquist-Johnson-Cook Model

In 1993 Holmquist, Johnson and Cook published a model with the purpose of developing a concrete model for impact computations, where the material experiences large strains, high strain rate and high pressure. Although the main purpose of the model was to simulate concrete, but it can be applicable for other materials. Due to the brittle behaviour of ice can be similar to concrete, this model can be appropriate.

Holmquist et al. (1993) described the material model and the determination of normalised constants. Finally they used a penetration computations and compared it with the test data. Seah (2006) goes through the parameters in more detail, and thereafter the same procedure for granite.

The Holmquist-Johnson-Cook (HJC) model contains a large number of material constants compared to simpler material models. In Table 2.1 the parameters are categorised into four groups; basic, strength, pressure and damage constants. The parameters with a star are normalised, which means that they are divided by the quasi-static uniaxial compressive strength σ'_c.

Numerous material tests are required to completely define the constants for a particular ice specimen. The strength model requires an unconfined compression test, a direct-pull test, a series of triaxial compressive tests, and a series of compressive tests at different strain rates. Due to lack of test data, the parameters in Section 3.3.3 may be obtained from tests that gives the necessary values.

Table 2.1: Material parameters for the HJC model

Basic Properties	Strength Model	Pressure-Volume Response	Damage accumulation
Mass density ρ	Uniaxial compressive strength σ_c'	Crushing pressure p_{crush}	Damage constant $D1$
Shear modulus G	Norm. cohesive strength A^*	Locking pressure p_{lock}	Damage constant $D2$
Poisson's ratio η	Norm. pressure hardening B^*	Crushing vol. strain μ_{crush}	Plastic strain ε^p_{min}
	Strain rate coef. C	Locking vol. strain μ_{lock}	Failure strain, FS
	Pressure hardening exponent N	Pressure const. K_1, K_2, K_3	
	Max. tensile hydrostatic pressure		
	Norm. max. strength S^*_{max}		

Norm. - normalised
Coef. - coefficient
Vol. - volumetric

The normalised equivalent stress is given by $\sigma^* = \sigma/\sigma'_c$, where σ is the actual equivalent stress. From the original paper, the specific expression for normalised equivalent stress is,

$$\sigma^* = [A^*(1-D) + B^* P^{*N}][1C^* \ln(\dot{\varepsilon})^*] \tag{2.16}$$

where the isotropic damage scalar D is given a value between 0 and 1, expressed in Equation 2.17. The dimensionless strain rate $\dot{\varepsilon^*} = \dot{\varepsilon}/\dot{\varepsilon_0}$, where $\dot{\varepsilon}$ is the actual strain rate and $\dot{\varepsilon_0}$ is the reference strain. A graphical representation of the HJC model is given in Figure 2.12.

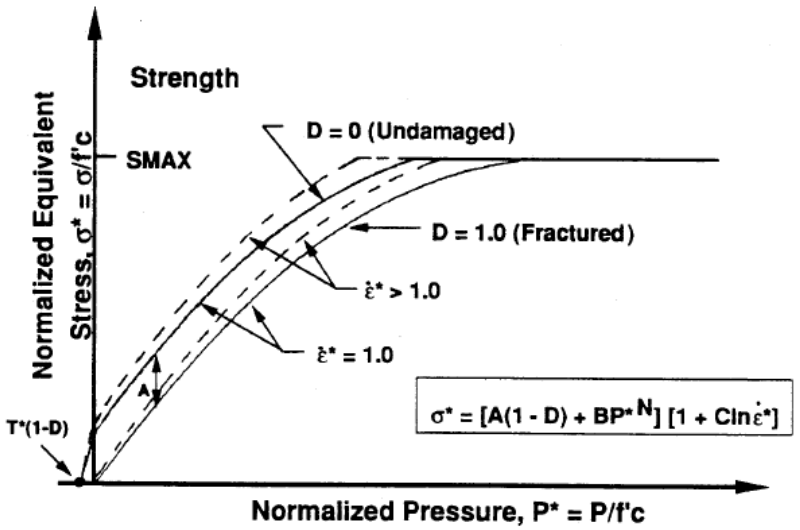

Figure 2.12: Strength response of the HJC material model. (Holmquist et al., 1993)

The HJC model is an elastic-viscoplastic model coupled with isotropic damage, where the response is separated into hydrostatic and deviatoric contribution. The model accumulates damage from both equiv-

alent plastic strain and plastic volumetric strain. It is expressed as,

$$D = \sum \frac{\Delta\varepsilon_p + \Delta\mu_p}{\varepsilon_p^f + \mu_p^f} \tag{2.17}$$

where $\Delta\varepsilon_p$ and $\Delta\mu_p$ are the equivalent plastic strain and plastic volumetric strain during loading, respectively. The denominator is the plastic strain to fracture under a constant pressure P, i.e. $f(P) = \varepsilon_p^f + \mu_p^f$ (Holmquist et al., 1993). The specific expression which follows, where D_1, D_2, P^* and T^* are presented in Table 2.1.

$$f(P) = \varepsilon_p^f + \mu_p^f = D_1(P^* + T^*)^{D_2} \tag{2.18}$$

From the equation above it is given that plastic strain to fracture increase with increasing normalised hydrostatic pressure P^*, but the material can not undergo any plastic strain at $P^* = -T^*$. Therefore a third constant ε_{min}^f is provided to allow a finite amount of plastic strain to fractured the material, as illustrated in Figure 2.13 (Holmquist et al., 1993).

The hydrostatic pressure-volume relationship is presented in Equation 2.19 and Figure 2.14. The figure illustrates three separated regions of the pressure-volume response. The first region is linear elastic and occurs at $P \leq P_{crush}$, the second region $P_{crush} < P \leq P_{lock}$ and the third region defines the fully dense material. The dense region is defined as $P > P_{lock}$, i.e. a fully compaced material where all air voids are removed.

The crushing pressure and volumetric strain are obtained from $p_{crush} = \sigma_c/3$ and $\mu_{crush} = p_{crush}/K$, respectively. K is the bulk modulus, and is defined in Equation 2.4.

$$P = K_1\bar{\mu} + K_2\bar{\mu}^2 + K_3\bar{\mu}^3 \tag{2.19}$$

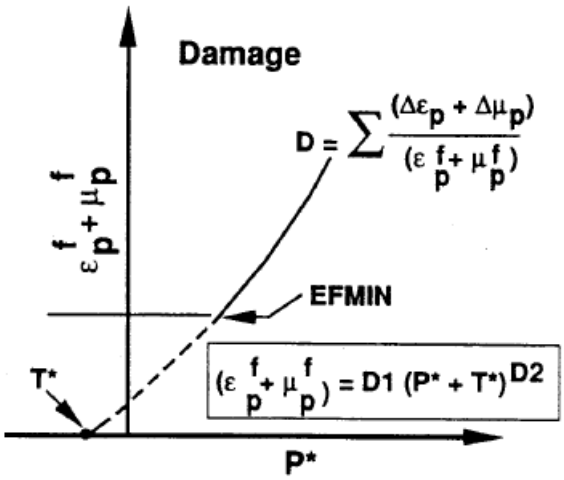

Figure 2.13: The damage of fracture of the HJC material model. (Holmquist et al., 1993)

where $\bar{\mu} = (\mu - \mu_{lock})/(1 + \mu_{lock})$ and K_1, K_2 and K_3 are material parameters that can be determined from Equation 2.20. Golding (2012) derived the constants to be determined in an easier way. The parameter S is the Hugoniot constant.

$$K_1 = \frac{E}{3(1-2\nu)} \qquad \text{for } P \leq P_{crush} \tag{2.20a}$$

$$K_2 = K(2S-1) \qquad \text{for } P_{crush} < P \leq P_{lock} \tag{2.20b}$$

$$K_3 = K(1-4S+3S^2) \qquad \text{for } P > P_{lock} \tag{2.20c}$$

To get a realistic solution, an erosion algorithm have to be used. In the HJC model the criterion of erosion is determined by using plastic failure strain FS. Unfortunately, the subject of erosion criterion was not described by Holmquist et al. (1993). Seah (2006) had a

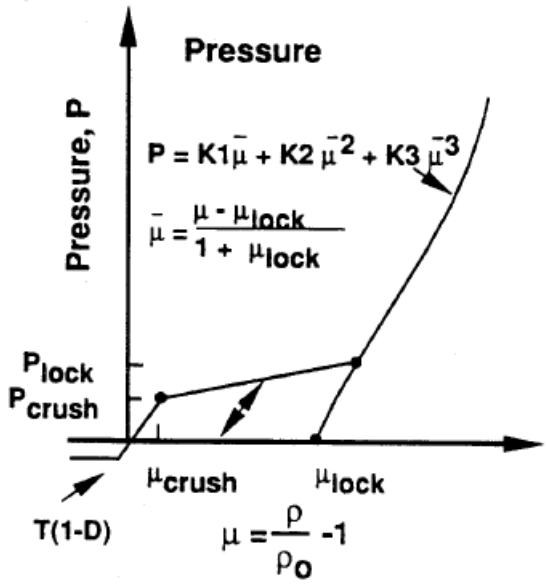

Figure 2.14: Pressure versus volume response for the HJC material model. (Holmquist et al., 1993)

parameter study for the erosion criterion, including a description of its behaviour.

If the erosion criterion is too low, the behaviour of the system will be inaccurate or even unphysical. For instance, the stress wave propagation and confined effects will be reduced since the strain energy can not be transmitted. Therefore, it is important that an accurate value of the erosion criterion FS is determined. In Chapter 4 different values of the parameters are compared.

Note that the term erosion in this context does not refer to the physical failure mechanism. According to Leppänen (2002) the erosion criterion is set above 1.5, and a parameter study by Johnson et al. (1998) concludes that erosion criteria for concrete above 3.0 will give realistic results. Seah (2006) conclude with the same value as Johnson et al. (1998) for both concrete and granite.

The softening behaviour of the considered material under uniaxial compression depends on the value of ε^f_{min}. According to Seah (2006) failure of the material can be delayed by adopting higher values of ε^f_{min}.

Due to the amount of parameters, further description is given together with the characterisation of the material model in Section 3.3.3.

2.7.4 Lemaitre Damage Model

The Lemaitre Damage model is based on the work of J. Lemaitre and J. Dufailly. The damage model is a pressure independent plasticity model with yield surface defined by the function $F = \sigma^v_y - \sigma_y = 0$, where σ^v_y is the equivalent von Mises stress and σ_y is the uniaxial stress (Hallquist, 2014).

Mass density ρ, Young's modulus E, Poisson's ratio ν, initial stress σ_{y0}, isotropic hardening modulus H, critical damage scalar D_c and damage material constants S and t need to be determined. The parameters for kinematic hardening are assumed neglected.

In the Lemaitre Damage model the hardening modulus affects the slope of the load-displacement curve beyond the linear-elastic section, and the critical damage parameter failure.

Equation 2.21 states the evolution of the isotropic damage value $\dot{D}$. The damage value is defined as a function of yield strength Y, the plastic strain $\dot{\varepsilon}_p$ and the material constants S and t.

$$\dot{D} = (\frac{Y}{S})^t \, \dot{\bar{\varepsilon}}^{pl} \tag{2.21}$$

In the keyword manual for LS-Dyna S and t have default values at $\sigma_y/200$ and 1, respectively. Damage accumulation begins when

$r > r_d$, where r_d is a damage threshold that can be determined from the plastic strain, since equation for damaged plastic strain r is also based on the plastic strain.

According to Lemaitre and Desmorat (2010), the critical damage value D_c is recommended to a range between 0.2 and 0.5 for most materials. Fracture occurs when isotropic damage scalar D reach the critical damage value D_c, and the element in the numerical analysis will be deleted.

A further description of the implementation of the equations in the model is listed in the keyword manual for LS-Dyna, Hallquist (2014).

2.8 Element Failure and Erosion Criterion

Many of the constituitive models in LS-Dyna do not allow failure or erosion. To give the element a failure or an erosion criteria, the keyword Mat_Add_Erosion is implemented in LS-Dyna. The keyword can also be applied to constitutive models with other failure or erosion criterion.

One of the numerical models is an interaction between a confined ice specimen and a spherically indenter, it is further explained in Section 3.2 together with the other numerical models.

The mentioned indentor must erode the surface of the ice specimen to obtain a brittle behaviour. Among the four material models mentioned above, the criterion is supplied to the Crushable Foam and the Brittle Damage model.

Each of the citerions defined in the keyword user's manual are applied independently. When a criterion is satisfied, the element will be deleted from the calculation.

In the material cards, there is not necessary to give a value for every single parameter. An exclusion number, EXCL, allows the user to specify criteria to be ignored without ambiguity. The cost of failure modes will then be reduced.

The criteria used for the actual material models, is the principle stress at failure σ_{max}, due to descriptions given earlier in this chapter. Failure occurs when the maximum principal stress reaches a critical value, $\sigma_1 \geq \sigma_{max}$ (Hallquist, 2014).

Chapter 3

Numerical Simulations

In this chapter, hardware and sofware used to the numerical simulation are presented, the numerical model set-up described and the parameters to each material model characterised.

The results from the simulations are presented in Chapter 4 and further discussed in Chapter 5. In the discussion some of the results from the numerical simulation will be compared with measurements from laboratory and in-situ experiments.

3.1 Hardware and Software

Two clusters were applied for the numerical analyses. The preliminary simulations, i.e. before the final analyses, were run at the cluster Snurre with symmetric multiprocessing (smp). It is a Linux based Cluster which belongs to Faculty of Engineering Science and Technology at Norwegian University of Science and Technology (NTNU). Snurre consists of five computational nodes, each equipped with 2 six-core Intel X5680 central processing units (CPUs) and 24GB of memory.

All final simulations were run at Vilje, a high performance supercomputer with smp and massively parallel processing (mpp). Vilje houses a total of 1404 computational nodes with 2 eight-core CPUs and 32GB of memory each. The system is procured by NTNU together with met.no and UNINETT Sigma.

The difference between smp and mpp is how the job utilize the available CPU cores. The "do loops" in the smp version will be distributed over a chosen cores, while the mpp version divide the numerical model into as many parts as there is cores specified.

The analytical software LS-Dyna V971 R7 was used, which is a 3D FEA non linear program for explicit time integration. LS-Dyna contains a number of contact algorithms and a large collection of material models that can be chosen for the interacting structures. This is an advantage when the most suitable material model for sea ice should be determined. The input data is prepared and results processed in the interactive program LS-PrePost.

The latest keyword user's manual is divided in two parts; one for the material models and one for the remaining keywords (Hallquist, 2014).

3.2 Numerical Model Set-up

There will be three numerical models presented in this section. The first is a single volume element, to easier understand the behaviour of each material model. The second model is the main numerical model, an indentation of a confined ice specimen. Finally, a numerical model with a drifting ice sheet towards an offshore structure are presented.

Some assumptions are made regarding the numerical simulations. Shear band, which is development of cracks, and extrusion of ice are not taken into account. Only ice under compression in the loading

direction is studied. The purpose is to see if the force-displacement curve gives the desired loading pattern that comes with brittle failure.

Figure 3.1 shows the numerical models. Note that they are not in the right scale in relation to each other.

3.2.1 Single Volume Element

For the single volume element a eight noded hexahedral element with full integration were used.

There is an advantage to use a single volume element, shown in Figure 3.1a, before the main analyses. The behaviour of each material model can be investigated with compressive or tensile loading. In this case the volume element is being compressed, due to the loading situation described in the next section. In the input file a easy load curve is given, which describe the compressive load.

In this case, it is desirable that the elements goes to failure. If not a ductile behaviour develops, and the characterised sawtooth pattern in brittle damage will not occur.

3.2.2 Confined Ice Specimen

The main numerical model in Figure 3.1b, is initially a small-scale laboratory ice-indentation test performed in Erland M. Schulson's laboratory conducted by Kim et al. (2012). Figure 2.6 shows the schematic sketch of the experimental setup. The initially tests were performed on confined and unconfined freshwater granular and columnar S2 ice at -10°C and -40°C.

In this context, the simulated test is confined S2 sea ice at -10°C using semi-spherical indenter (hemispherical-ended rods). The radius

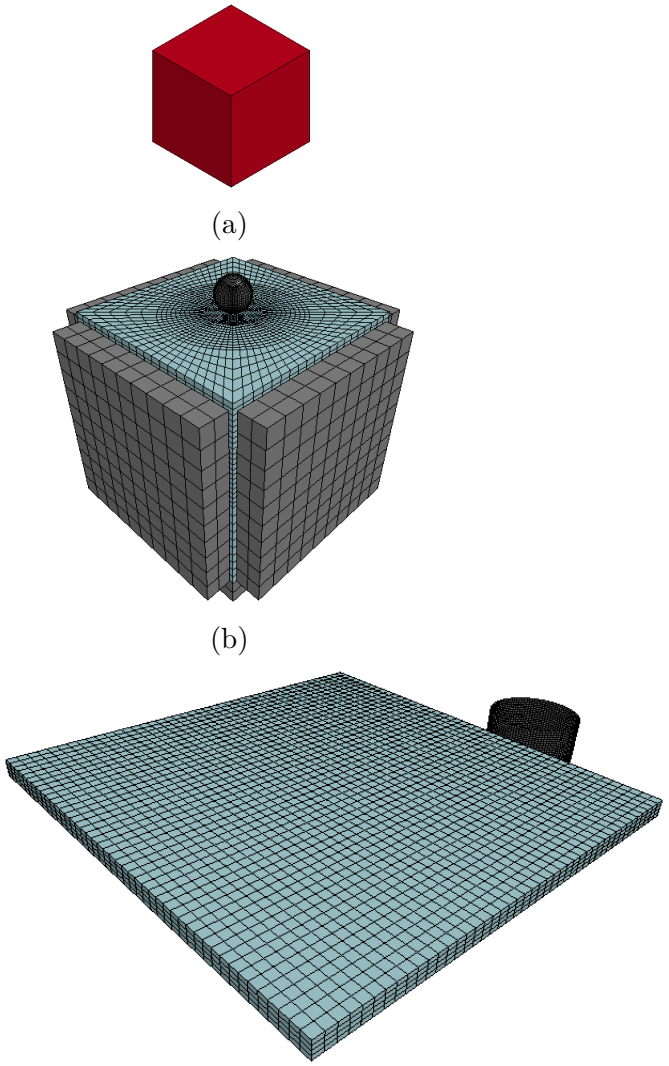

(a)

(b)

(c)

Figure 3.1: The numerical models; (a) Volume element, (b) Interaction between a confined ice specimen and an indenter (c) Drifting ice sheet toward an offshore structure.

of the indenter is 12.7 mm, and the constant penetrate velocity and depth are 5.08 mm/s and 12.7 mm, respectively.

The ice specimen is confined with aluminium extenders whit measurement at 140x140x20 mm^3, while all edges of the ice specimen is determined to 146 mm. The numerical simulation has similar properties and set-up like the tests EK7 and EK8 from the laboratory. See section Figure 2.6 for test set-up and Figure 2.7 for the results.

The ice specimen is confined to simulate a similar behaviour like an ice floe. If a small piece of an ice floe is taken into account, this piece will be sourrounded by ice. The confined situation will then illustrate a piece from a ice floe in a good way, i.e. triaxially loading.

Eight noded hexagonal solid elements with reduced integration is employed for all parts of the model. The ice specimen consists of 4800 solid elements. The finite element model for the indenter and the five plates are treated as rigid bodies.

In order to align the numerical model with the ice physics, there is assumed an element size like the grain size under the loaded area at the ice specimen (von Bock und Polach and Ehlers, 2013). The grain size ranges from 1 mm to 2.4 mm for the ice specimen in the laboratory test described above. Note that the mesh density of the ice decrease from the centre to the outher, which apply for all directions of the cube, i.e. horizontally and vertically.

The surface contact algorithm in LS-Dyna is used to define contact between the ice specimen and the plates are Contact_Automatic_-Surface_to_Surface. The contact between the indenter and the ice specimen is Contact_Eroding_Surface_to_Surface. The ice is the master, then the other parts will be the slave. The time step for the simulation is determined when the simulation has started.

Energy Control

Explicit non-linear analyses with reduced integration, must be controlled for hourglass energy, energy balance and kinetic energy. All values are found from the ASCII file, GLSTAT. The energy check is perfomed to warn against possible numerical instability, spurious modes.

The hourglass method is chosen to be type 6. In the keyword control_energy HGEN is set to 2. The hourglass energy is then calculated.

Hourglass mode has to be minimized, and as a rule-of-thumb hourglass energy should be less than 10 % of the peak of the internal energy. It can be controlled in Control_Hourglass by regulate the QH if the rule is not satisfied. Recommended value for solid element is 0.1 or less. All hourglass is elastic, lower QH can cause a more plastic consideration.

The energy balance is perfect if the total energy is equal to the sum of initial total energy and external work. In LS-Dyna this is controlled by the energy ratio. The energy balance is sufficient if the energy ratio is equal or close to 1. The energy ratio is the total enegy divided by initial energy and external work.

The last control is to see if the kinetic energy is held at a minimum.

3.2.3 Ice Sheet Towards an Offshore Structure

The final numerical model is developed by Hilding et al. (2012). It is a full scale simulation of an ice sheet drifting towards an offshore structure. The results from these simulations are compared with a full scale measurements of ice forces from the lighthouse Norströmsgrund in the Gulf of Bothnia. The measurements from the lighthouse is

given in Figure 4.16. The results from the numerical simulations are presented in section 4.3 and further discussed briefly in section 5.2.

The methodology is based on cohesive element method to model the ice fracture in conjunction with a homogenisation method, which is developed by Hilding et al. (2012). The homogenisation method is used to capture sub element size cracks in a cost effective manner. The crack propagates when the cohesive elements have deformed sufficiently, then the element goes to failure.

In the numerical model it is looked at an ice fracture called continuous crushing mode. In this fracture mode the ice breaks and get crushed into very small fragments, <1cm, during the interaction with the structure. The crushed ice accumulates both below and above the ice sheet.

The lighthouse is modelled as a rigid body, and the ice sheet is 0.69 m thick with element size at 0.13x0.2x0.2 m· The shear and tensile strength for vertical cohesive elements is 1 MPa, while it is 1.1 MPa for horizontal cohesive elements. The contact algorithm Contact_-Eroding_Surface_To_Surface has been used between the ice and the lighthouse. Each analysis where terminated after 5 seconds.

3.3 Characterisation of the Material Model

In Section 2.7 the theoretical aspect for each material model was presented. The following sections characterise the parameters for the material models. The parameters are determined during litterature study in Chapter 2, assumptions and inverse modelling.

As stated earlier, ice is a complicated material. The ambition with the numerical simulations are not to develop a material model which captures the behaviour of ice in all respects. The most important is to develop the brittle behaviour under triaxial loading, and to get

the sawtooth pattern in a force-displacement curve.

Three material parameters recurs in the material models. They are determined from the theory chapter, Chapter 2. The Young's modulus E and the Poisson's ratio ν are determined to be 8 GPa and 0.33, respectively. In Section 2.1.2 the mass density is chosen to 900 kgm^{-3}.

3.3.1 Crushable Foam Model

The material properties for the Crushable Foam model are the density ρ, Young's modulus E, Poisson's ratio ν, the tensile cutoff σ_t^c and the load curve defining yield stress versus volumetric strain. Poisson's ratio is assumed to 0.003, since a low value is recommended according to Section 2.7.1. The reason is to insure a flattening that reminiscent of melting. The parameters are presented in Table 3.1.

Table 3.1: Summary of parameters used in Crushable Foam model

ρ $[kg/m^3]$	E $[GPa]$	ν -	lcid -	σ_t^c $[MPa]$	Damp. -	σ_{max} $[MPa]$
900	8	0.003	see Figure 3.2	0.65	0.5	Section 4.2.1, Results

The volumetric strain is the unit change in volume due to a deformation. In this context compression is a positive value. The load curve for the yield stress versus volumetric strain is given in Figure 3.2. The values are obtained by Gagnon (2011).

The four point in the high stress curve are 0.0, 0.0; 0.015, 25.0×10^6; 0.5, 50.0×10^6; and 1.0, 50.0×10^6, where each pair corresponds to fractional volumetric strain and yield stress respectively. For the other

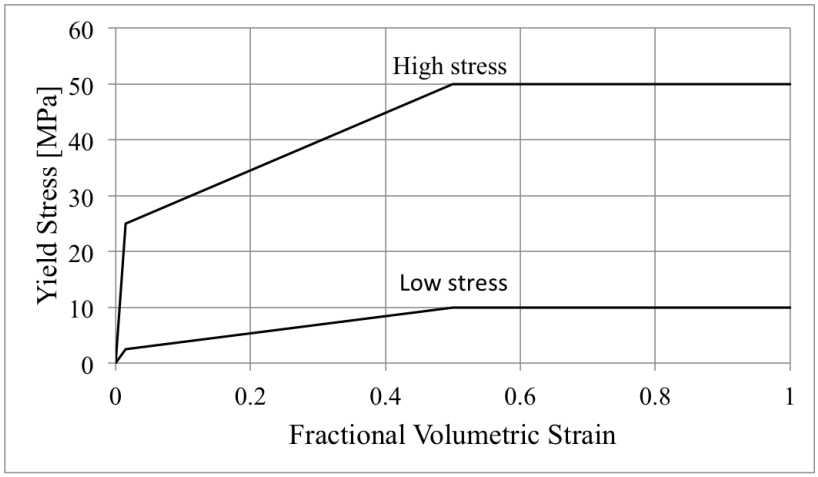

Figure 3.2: Yielding stress versus volumetric strain curves for Crushable Foam model. Data from Gagnon (2011).

curve, low stress, the points defining the curve are: 0.0, 0.0; 0.015, 2.5×10^6; 0.5, 10.0×10^6; and 1.0, 10.0×10^6. Note that Gagnon (2011) combined the curves in his simulations, here they will be considered seperately.

To simulate the numerical model with Crushable Foam model, the erosion/failure criterion described in Section 2.8 was applied. The criterion should improve the existing model to avoid bad element shapes, which can occur due to compressive deformation in ice as a foam.

3.3.2 Brittle Damage Model

The determined ice parameters for the Brittle Damage model are given in Table 3.2. The parameters are the density ρ, Young's modulus E, Poisson's ratio ν, tensile strength σ_t, shear strength σ_s, fracture toughness G_c, shear retention β, viscosity η and compressive

yield stress σ_y.

Fracture toughness and viscosity are important for the stability of the calculation. The fracture toughness is chosen to 115 kPam$^{0.5}$, then the toughness G_c is calculated from Equation 2.7. For ice the value of shear retention should be a small value, and are estimated to 0.016. From the recommended values of the viscosity in Section 2.7.2, it is chosen to be 0.724 J/m^2.

Due to a problem with the penetration according to this material model, the erosion/failure criterion in LS-Dyna were used for Brittle Damage model. Different values for the maximum compressive stress σ_{max} with respect to the comparison.

Table 3.2: Summary of parameters used in Brittle Damage model

ρ $[kg/m^3]$	E $[GPa]$	ν -	σ_t $[MPa]$	σ_s $[MPa]$
900	8	0.33	0.65	0.7
G_c $[J/m^2]$	β -	η $[MPas]$	σ_y $[MPa]$	σ_{max} $[MPa]$
1.5 7.1	0.016	0.724	8	Section 4.2.2, Results

3.3.3 Holmquist-Johnson-Cook Model

The Holmquist-Johnson-Cook (HJC) model is presented in Section 2.7.3. In this section the characterisation of the parameters are organised in basic properties, strength, pressure-volume response and damage accumulation parameters.

A summary of the material parameters is given in Table 3.3, the descriptions of each term is given in Table 2.1. The unconfined compressive strength is σ_c'=8 MPa, which is the value the normalised constants have been divided by.

Table 3.3: Summary of parameters used in HJC model

ρ $[kg/m^3]$	G $[GPa]$	A^* -	B^* -	C -	N -	$\sigma_c^{'}$ $[MPa]$
900	4.96	0.0461	1.2930	0.0097	1.0290	8
T $[MPa]$	ε_0 -	ε_{min} -	S^*_{max} -	p_{crush} $[MPa]$	$\varepsilon_{vol.crush}$ -	p_{lock} $[MPa]$
0.65	1	0.100	3.375	2.67	0.0004	2.67
$\varepsilon_{vol.lock}$ -	D_1 -	D_2 -	K_1 $[GPa]$	K_2 $[GPa]$	K_3 $[GPa]$	FS -
0.0	0.02 0.04 0.164	1.0	6.667	0.800	0.872	0.1, 0.7 1, 1.5, 2

Basic Properties

The basic properties, density, Young's modulus and Poisson's ratio, are the same as for the other material models. However, this model requires a shear modulus G, which is calculated from the Poisson's ratio ν and Young's modulus E, see Equation 2.3. The shear modulus G is calculated to be 4.96 GPa. In the numerical results, the Young's modulus is compared with the shear modulus in a force-displacement history.

Strength Model Parameters

The next step in the characterisation of the parameters are the strength constants, A^*, B^*, C, N, S_{max} and T.

The maximum strength is assumed to 27 MPa, which gives a normalised maximum strength S_{max} at 3.375. From Section 2.2.2, the tensile strength can be determined to 0.65 MPa.

The remaining strength parameters are found using results from the triaxial compression test by Golding (2012). There is given a log-log plot of maximum effective stress versus applied strain for columnar ice deformed under (1.0:R_{21}:R_{31})=(1.0:0.5:0.2) at -10°C. Due to lack of access to the test measurements, the values are obtained from the mentioned graph. Table 3.4 gives the results from the triaxial compression test by Golding (2012), and the results from the calculation to determine the upcoming values.

The third column in the table given below with the stress σ_{11} in X_1 direction is calculated from Hill's criterion, Equation 2.10. The effective failure stress σ is given as the σ_y^M in the equation.

The uniaxial failure stress are determined to $\sigma_{u,1}^f = 32.5$ MPa and $\sigma_{u,13}^f = 19$ MPa for the angles 0°and 90°, respectively (Schulson and Duval, 2009). The remaining values are replaced with $\sigma_{22} = 0.5\sigma_{11}$ and $\sigma_{33} = 0.2\sigma_{11}$. Finally the equation of Hill's criterion can be reorganised, and the stress σ_{11} in X_1 direction is determined. The directions of the stresses σ_{11}, σ_{22} and σ_{33} is given in Figure 2.4.

Together with the proportional loading path and results from Hill's criterion the hydrostatic pressure P can be calculated from Equation 2.12. The hydrostatic pressure and effective stress at failure are normalised with the uniaxial compressive stress σ_c'=8 MPa, and given in the two last columns.

The normalised hydrostatic pressure and the normalised effective failure stress in Table 3.4 are given in Figure 3.3. From this figure the

Table 3.4: Development of pressure and stress to the HJC model

Eff. Failure stress σ $[MPa]$	Applied strain $\dot{\varepsilon}_{11}$ $[s^{-1}]$	Stress in X1 σ_{11} $[MPa]$	Hydr. Pressure P $[MPa]$	Norm. Hydr. Pressure P^* $[MPa]$	Norm. Eff. Failure Stress σ^* $[MPa]$
4.446	8e^{-6}	5.838	3.308	0.414	0.556
7.112	1.9e^{-4}	9.339	5.292	0.662	0.889
11.860	0.001	15.574	8.825	1.103	1.483
23.440	0.01	30.780	17.442	2.180	2.930
27.797	0.0211	36.502	20.684	2.586	3.475
21.528	0.0306	28.269	16.019	2.002	2.691
23.440	0.0348	30.780	17.442	2.180	2.930
22.490	0.037	29.533	16.735	2.092	2.811

normalised cohesive strength A* is determined.

The cohesive strength is defined as the difference between the undamage strength and the completly fractured strength at a given pressure. The intersection point at the ordinate, by the normalised stress σ^*, the A* is determined to be 0.0461. Note that the graph start from the normalised tensile strength at the abscissa, $T^* = 0.65MPa/8MPa = 0.08125$.

The strain rate coefficient C is obtained by performing *a least square fit* of the four data point shown in Figure 3.5. To obtain the strain rate effect alone, the pressure effect must be removed.

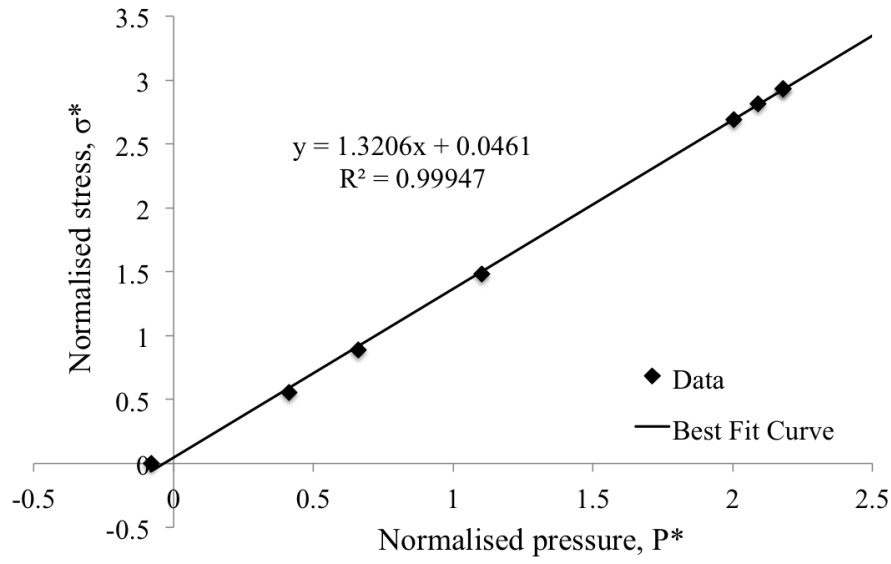

Figure 3.3: Description of the strength model for sea ice for finding A^*.

The technique to determine the strain rate coefficient C is given in Figure 3.4 and 3.5. The first figure gives the normalised effective stresses versus the normalised pressure at different strain rates. The four strain rates are found from Table 3.4. A straight line is drawn from the maximum normalised tensile hydrostatic pressure T^* through each of the test data.

The change in strength due to strain rate alone is determined at a constant normalised pressure P^*=1.1, corresponding to the data at ε=0.001. The ε is an assumed limit between ductile and brittle failure. The intersection points at P^*=1.1 for the four graphs are used further in Figure 3.5.

The last parameters, B^* and N, are determined by fitting the curve using the least squares method in Matlab. The constants are de-

fined from the equation 2.16, where $\dot{\varepsilon}^* = 1.0$. Hence, B^*=1.239 and N=1.029.

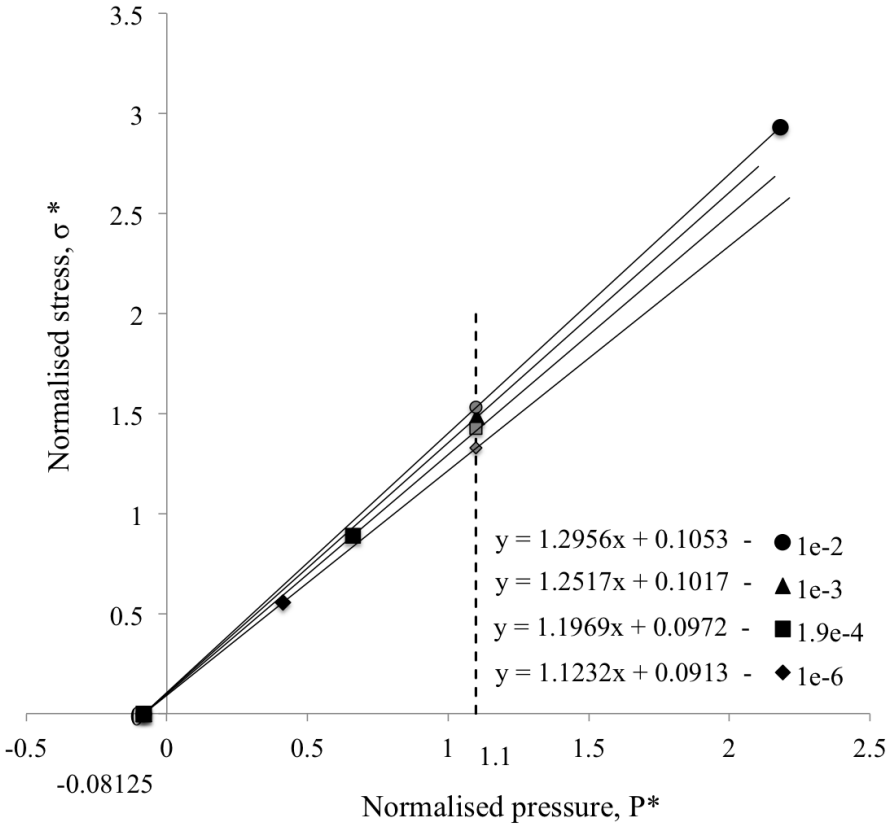

Figure 3.4: Normalised effective stress versus normalised pressure at different strain rates.

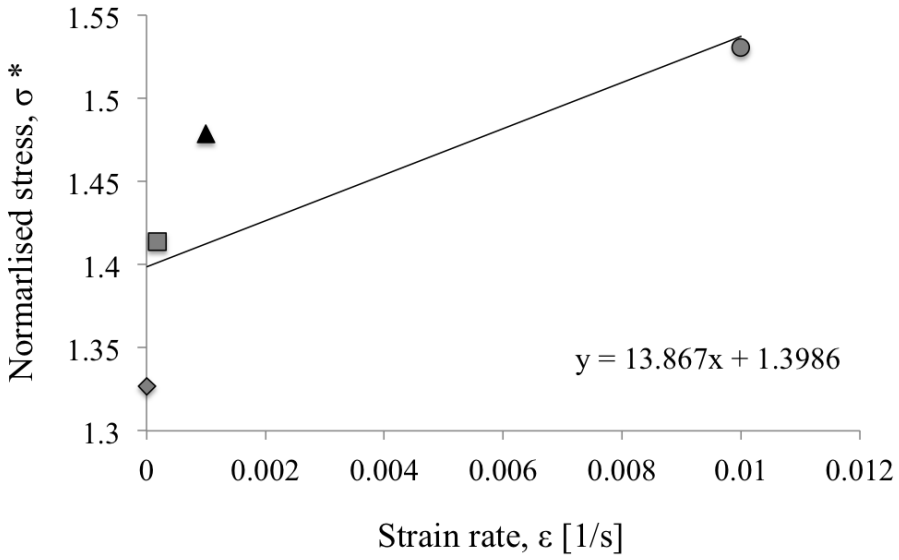

Figure 3.5: Determinition of normalised parameter C*.

Pressure-Volume Response Parameters

Due to lack of information in the transition region of the pressure-volume response curve, μ_{lock} is set to 0 and p_{lock}=p_{crush}=2.67 MPa. The equation of p_{lock} is presented in the theory part of this model, and the crushing pressure μ_{crush}=0.0004.

From Equation 2.20 the parameters K_1, K_2 and K_3 can be determined. The Hugoniot data is not available for ice, hence a material that resemble the material properties of ice is used. There is assumed to be acceptable if the density is closely matched. The pumice is chosen, it is a volcanic rock that intially float in water and has a density at 550 kg/m^3. The Hugoniot constant S is 1.06. This assumption only affects the constants for equation 2.19 and the high-pressure behaviour of the material.

Damage Accumulation Parameters

The damage constants D1 and D2 and the plastic strain ε^p_{min} require results from a cyclic compressive loading.

Due to lack of information, results from a biaxial test conducted by Iliescu and Schulson (2002) is used to find ε^p_{min} and a normalised pressure P^*. Note that this P^* is not the same as above.

The relation $\sigma_{22} = R\sigma_{11} = 0.072 \pm 0.012\sigma_{11}$ is assumed to also apply for the strain rate when finding ε_{22} from ε_{11}. The equivalent plastic strain rate is then obtained from Equation 3.1 to be ε^p_{min} =0.07203.

Since $P = (\sigma_{11} + \sigma_{22})/3$ for biaxial loading, the normalised value is P^*=0.2698. Finally D1 can be determined to 0.164. According to Holmquist et al. (1993) D2=1, the same value is used here. The constant D1 is determined from the Equation 2.18.

$$\bar{\varepsilon} = (\frac{2}{3}(\varepsilon^2_{11} + \varepsilon^2_{22}))^{0.5} \tag{3.1}$$

Since the D1 is sensitive to the selected strain rate, another value is also calculated for ice. For an uniaxial loading with plastic strain at 0.01 and normalised pressure $P = (\sigma_{11}/3)/\sigma'_f$=0.4146. That leads to another damage constant, D1=0.02. Holmquist et al. (1993) determined the damage constant D1 to be 0.04 for concrete, which will be compared with the two calculated above in a force-displacement history together with the results.

The failure strain, FS, is determined due to inverse modelling. It is important to chose a correct value for failure strain, if not uncorrect values will be plottet and elements may blow up. In this context there will be tried five values; 0.1, 0.7, 1, 1.3 and 2.

3.3.4 Lemaitre Damage Model

This model requires few parameters, the density ρ, Young's modulus E and Poisson's ratio ν is the values presented in the introduction of this section. The other parameters are determined by assumption, scaling and default values.

Table 3.5: Summary of parameters used in Lemaitre Damage model

ρ $[kg/m^3]$	E $[GPa]$	ν -	σ_{y0} $[MPa]$	H $[MPa]$	β -	S -	T -	DC -
900	8	0.333	1	61.6	1	5000	1	0.200 0.350 0.500

The initial yield stress σ_{y0} is a assumed value. The isotropic hardening modulus H is scaled from the paper by von Bock und Polach and Ehlers (2013), where a value for Young's modulus and hardening modulus for ice is already given.

Default values are chosen for the isotropic hardening parameter β and the damage constants S and t. The critical damage value D_c was determined by chosing values between 0.2-0.5, and see how dependent the analyses are of the parameter. The kinematic hardening parameters are neglected.

The isotropic damage flag, output stress flag and damage plastic strain are set to, respectively, 1, 0, 1. The damage threshold r_d were assumed to zero, the value depends on when damage accumulation begins, $r > r_d$. Since it is zero, damage depends on the damage plastic strain r. More about these in the keyword manual by Hallquist (2014).

Chapter 4

Numerical Results

In this chapter, the numerical results obtained from the analyses are given. The numerical models are presented in Chapter 3, and illustrated in Figure 3.1.

Before the main numerical model, a single volume element were taken into account. It was used to understand the behaviour of the material models. Here the results are briefly presented.

In Section 4.2 the results from the confined ice specimen with an indenter is presented. This is the most important part of the chapter, since the input parameters for each material model are investigated. The results are given in figures that compare the force-displacement history. They are essential to the comparison within and between the material models. If the results from the material models are sufficient according to the brittle behaviour, a desired sawtooth pattern is shown. More about the brittle failure and the desired sawtooth pattern in Section 2.3.

How the indenter penetrates the ice specimen may be related to the graphical results. Four tables with the first principal stress presented by iso-plots are given as a final presentation of the numerical model

of the indenter and the confined ice specimen.

At the end the results from the drifting ice sheet developed by Hilding et al. (2012) are presented. The material models are compared with the original material model in a force-displacement diagram and with illustrative figures from the simulations at termination time.

The numerical simulations are runned with both smp and mpp version of LS-Dyna, which are described in Section 3.1. The CPU time for analyses runned with mpp version was less than those with smp version.

For some of the models, the same analysis gave different results running smp and mpp. Hence the computational time is not further considered, just commented.

Were the smp and mpp version gave different results, a comparison is conducted. The smp version should give the same results if there is used one or eight cores, while the mpp version can give different results depending on the number of cores.

4.1 Results: Single Volume Element

The time step of the single volume element increased for Crushable Foam, Brittle Damage and Lematire Damage model under compression, i.e. the element was not deleted. For the latter model the elemtents will be deleted by a numerical model, because of a damage constant and the elements will affect each other. The two other have to be further studied in terms of element failure in compression. As described in Section 3.3 were the parameters are characterised, the Mat_Add_Erosion are presented.

For the HJC model it was noticed that the deletion time for the element depends on the plastic strain ε_{min} and the erosion criterion FS. If erosion criterion was unchanged and the plastic strain was

set to a high or low value, it was seen that the elements were deleted faster by a higher value of plastic strain. However, a constant plastic strain and variation in failure strain gave an earlier deletion of the element with low failure strain values. This is presented in Figure 4.8 for the numerical model with the confined ice specimen.

The deletion time was not affected by changes according to the reference strain ε_0. Therefore the value from the original paper by Holmquist et al. (1993) at 1.0 is used in all analyses.

4.2 Results: Confined Ice Specimen

The results from the confined ice specimen are given as a graphical view of the vertical force versus the displacement caused by the indenter. The parameter study will be in focus, where chosen parameters with different values are compared against each other. The considered parameters are chosen for the reason that they may have an effect on the brittle failure in sea ice.

The interaction between the indenter and ice specimen, deletion of elements, is shown by a iso-plot with a fringe lever in section 4.2.5. The iso-plots are given for the first principal stress.

During the presentation of each comparison in the figures, some comments regarding the results are given to conclude which parameters that is taken further into account. In Chapter 5 the material models are further discussed and compared to each other.

Explicit non-linear analyses with reduced integration have to undergo an energy control. For the presented results, the hourglass energy, energy balance and kinetic energy are controlled.

The hourglass energy was satisfying for all analyses according to the rule-of-thumb presented in Section 3.2.2. For some cases the hourglass coefficient QH was reduced from 0.1 to 0.06. There were no

significant signs to spurious modes, since the energy ratio was approximately 1 for all analyses. The kinetic energy was also controlled, and the values was held at a minimum.

As a control if the results are approximately satisfying, the uniaxial stress under the indenter is calculated with the equation $\sigma = F/A$. Where, F is the vertical force and A is the penetrated area of the indenter by the peak force.

4.2.1 Crushable Foam Model

There was minimal problems regarding the analyses with the Crushable Foam model. The most demanding task was to determine the loading curve, yield stress versus volumetric strain. Therefore, the high and low stress curves from Gagnon (2011) was used, see Figure 3.2. The rest of the chosen parameters are given in Table 3.1.

The force-displacement curves below show that the Crushable Foam model depends on the damping constant, Poisson's ratio and the loading curve. The tensile cutoff is essential due the correct loading path. In Figure 4.3 the finaly plot of the force-displacement is viewed with high and low stress curve.

The comparison of two damping coefficients, 0.1 and 0.5, shows that the brittle failure develop earlier when the damping coefficient is low. The lowest recommended damping coefficient at 0.05, did not pass the analysis. The time step increased, due to blown up elements.

In Figure 4.2 three graphs are plotted, with different value of Poisson's ratio and the tensile cutoff. The Poisson's ratio is given a low value, according to Gagnon and Wang (2012), and the true value of Poisson's ratio is determined earlier. Those values are 0.003 and 0.33, respectively. The latter ratio gives greatest forces, but a delayed element failure. Since there is recommended to use a low value for the Poisson's ratio, 0.003 have been used further.

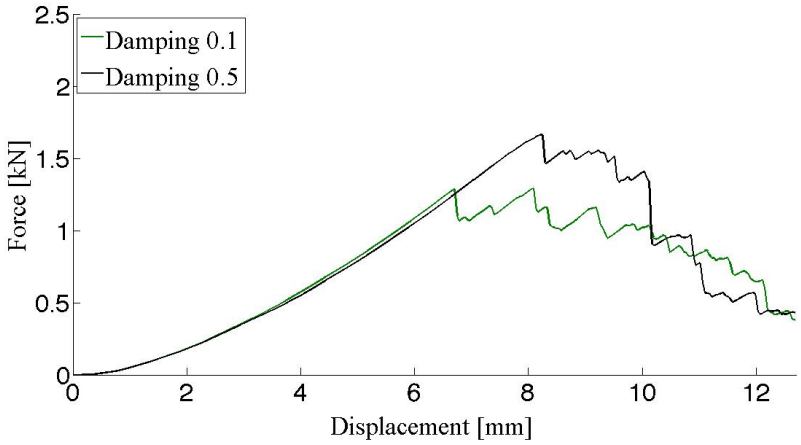

Figure 4.1: Crushable Foam model with various damping values, $\nu = 0.003$ and $\sigma_t^c = 0.65$ MPa.

To get reliable results the tensile cutoff σ_t^c have to be a nonzero positive value, which is a recommendation according to Hallquist (2014). The green graph given in Figure 4.2, along the abscissa, shows why the tensile cutoff should be a nonzero value.

Figure 4.3 view the finally results of the numerical simulation with the Crushable Foam material model. Note that the high stress curve is for unbroken ice, and low stress is for the crushed ice. The loading curve for high stress increase more rapid compared with the other curve. The vertical force dampens out after the maximum force is reached.

In the last figure the penetration depth for high stress and low stress by the peak forces 3 kN and 1.7 kN are 5.4 mm and 8.2 mm, respectively. This cause uniaxial stresses at 33 MPa and 8 MPa, as explained in the introduction of this section, which is satisfying compared to the section about compressive strength, Section 2.2.1.

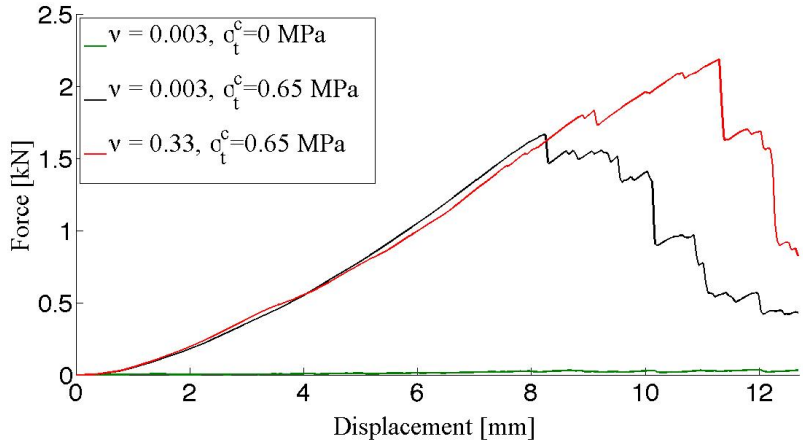

Figure 4.2: Crushable Foam model with various values for Poisson's ratio and tensile cutoff. Damping=0.5.

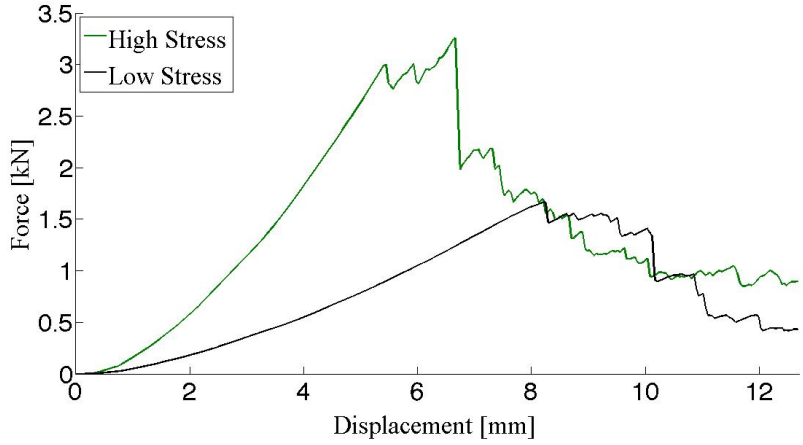

Figure 4.3: Crushable Foam model with high stress and low stress loading curve. Damping=0.5.

4.2.2 Brittle Damage Model

To determine the parameters given in Table 3.2 to the Brittle Damage model was simple, but a way more difficult to get the analysis to run normal. In the theory of the model, it is described that the elements will erode when the maximum stress is reached. In this case, the results then viewed a ductile behaviour with the material model alone. Hence, the erosion/failure criterion was added. The σ_{max} refer to the maximum principal stress in the material card to the Mat_Add_Erosion.

A ductile behaviour occured when $\sigma_{max} > \sigma_0$, i.e. the principal stress was given a higher value than the compressive yield stress in the material card to the Brittle Damage model. If the opposite is the case, the elements eroded by failure.

There were tried to run analyses with viscosity parameters outside the range 0.71 to 0.73, but error occured. Those results viewed that the recommended values for the viscosity is prefered. Several analyses were run with both smp and mpp version for comparision, since both gave different results. The smp and mpp version are described in Section 3.1.

The figures 4.4 and 4.5 view the difference between the smp and mpp version. The first figure, with G_c=1.5 J/m^2 and σ_{max}=3 MPa, have almost the same path and force drops at same penetration depth. The most significant difference is for the second figure, where the first force drop with smp version is at 7.4 mm and mpp version gives a drop at 2.7 mm penetration depth. The maximum vertical force is 4.2 kN and 3.3 kN, respectively. This leads to a calculated uniaxial stress at for 24 MPa and 144 MPa for the smp and mpp version, respectively. Compared with the uniaxial strength given in Section 2.2.1, the results from the smp version is most realistic.

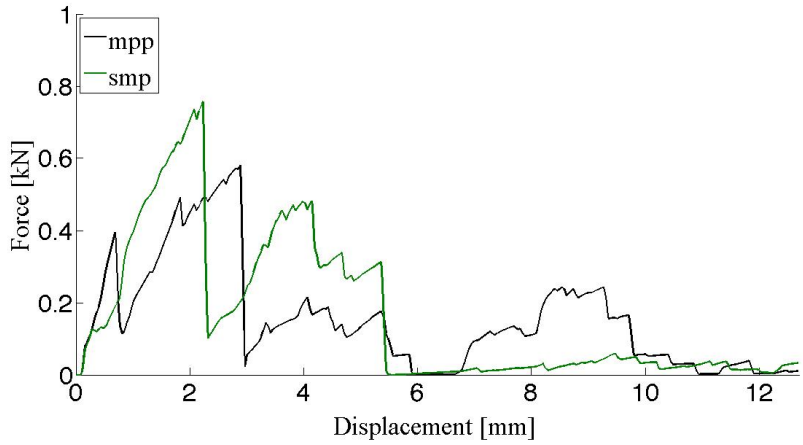

Figure 4.4: Brittle Damage model run with smp and mpp, G_c=1.5 J/m^2 and σ_{max}=3 MPa.

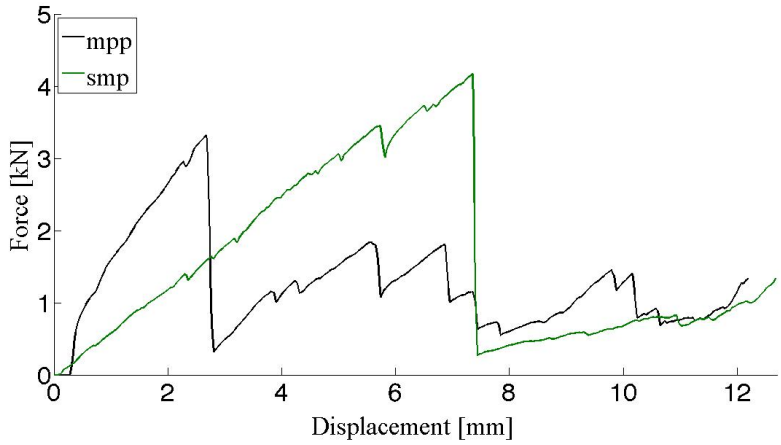

Figure 4.5: Brittle Damage model run with smp and mpp, G_c=7.1 J/m^2 and σ_{max}=8 MPa.

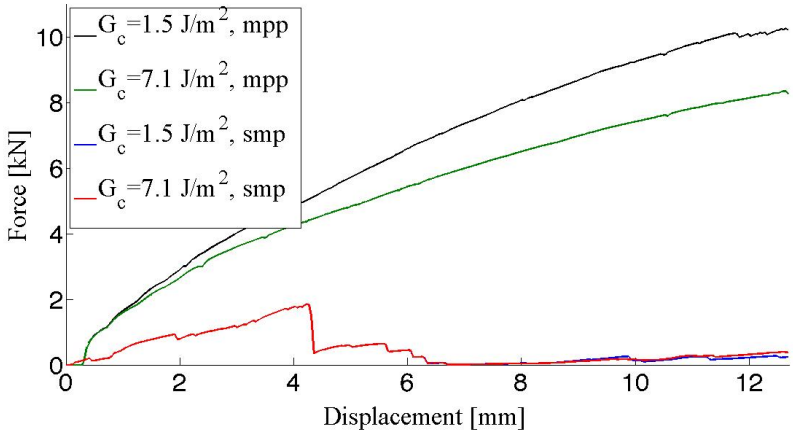

Figure 4.6: Brittle Damage model with various toughness and maximum stress. G_c=1.5 J/m^2 versus G_c=7.1 J/m^2 with σ_{max}=10 MPa and σ_{max}=5 MPa for mpp and smp version, respectively.

It seems to several elements fails simultaneously when the indenter penetrates the surface of the ice specimen, which causes a gap between the surfaces. From the force-displacement history this is viewed by the big drop in force value. The iso-plot in Table 4.3 gives a better view of the element erosion.

By a comparison of the toughness energy G_c, there is minimal differences. Figure 4.6 gives the graphs for two pair of comparisons, where the analyses with smp version have maximum stress σ_{max}=5 MPa and the mpp σ_{max}=10 MPa. The latter got a ductile behaviour, the reason might be that $\sigma_{max} > \sigma_0$.

To be noted, several analyses were run with different values below 0.1 for shear retention, but it had no significant effect on the results.

4.2.3 Holmquist-Johnson-Cook Model

There were many parameters that needed to be determined for the HJC model, a summary is given in Table 3.3. The most demanding part, where to find the parameter that determined the element erosion by failure. Parameters that were not found in litterature or by calculation, were found by using inverse modelling. Further, different compared values of the parameters presented and commented.

The damage constant D1 is sensitive to the value of plastic strain, which can be seen from Equation 2.17. Holmquist et al. (1993) gave a damage value D1 equal to 0.04 for concrete. In Section 3.3.3 two values to the respect to ice are calculated to 0.02 and 0.164. From the Figure 4.7 it is clearly shown that the damage constant should be in the range of 0.04 to get the desired behaviour.

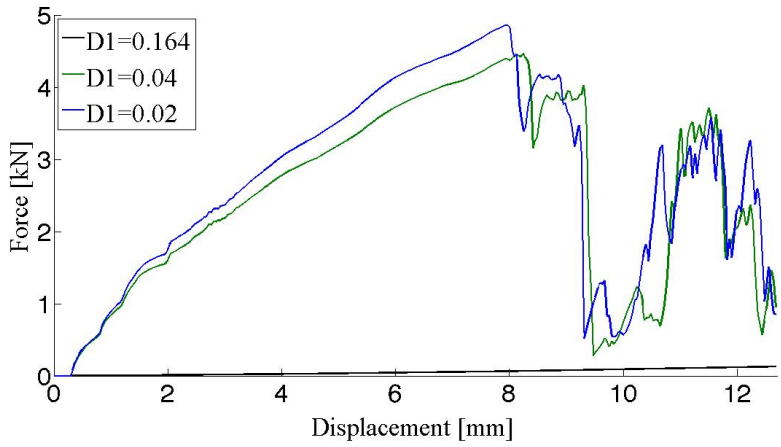

Figure 4.7: Three various values for damage constants, D1=0.164 and D1=0.02 are calculated and D1=0.04 from Holmquist et al. (1993). Shear modulus G and erosion value FS=1 are applied.

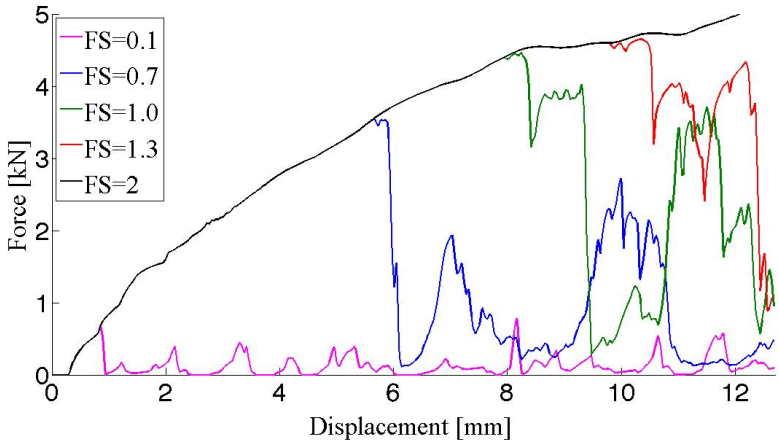

Figure 4.8: Determition of the erosion criterion FS. Shear modulus G and damage constant D1=0.04 are applied.

In Figure 4.8 five values are compared for FS, and the failure occurs earlier by an lower value. Which was the same as the study from the single volume element showed. The graph is plotted with a chosen damage constant D1=0.04 and the shear modulus G.

Each result from the analyses have the same slope and a ductile behaviour before failure. As described in Section 2.7.3, the erosion criterion is a fictive value and can not be determined from litterature. Inverse modelling has to be used to find a reliable value. In Section 2.7.3 it is mentioned that it is recommended to determine an erosion criterion above 1.5, it seems that is not the case for ice.

In the theory section for the HJC model there is mentioned that the erosion criterion can not be too low, which can give innaccurate or unphysical results. This statement are proven by a erosion criterion at 0.1 in Figure 4.8. For S2 sea ice the erosion criterion can be determined approximately in a range between 0.7 and 1.3.

Since the penetration depth is 12.7 mm, there is difficult to say some-

Table 4.1: Values for the von Mises and Hill's criterion

	von Mises	Hill
A^*	0.0357	0.0461
B^*	1.004	1.293
C	0.0142	0.0097
N	1.022	1.023

thing about the force-displacement curve of when FS is equal to 1 will continue. But as long as the vertical force increase after a drop for the values 0.7, 1.0 and 1.3, it also seems to be the same case for higher values of the failure strain.

In Section 2.6 it was defined that the von Mises yield criterion applies to granular ice and Hill's yield criterion to columnar ice. Since Hill's criterion requires some more parameteres, it is of interest to compare results from both methods. The different values between the criterions, are presented in Table 4.1. The parameters for von Mises are found in the same way as for Hill's.

There is seen from Figure 4.9 that the von Mises yield criterion gives lower values for the vertical force compared to Hill's criterion, which means that ice get a weaker behaviour. The values for the vertical force from the analysis with Hill's criterion, is almost 100 % higher than for the von Mises criterion. Note that the damage constant D1 is equal to 0.04, and that the shear modulus G is used.

Some places the Young's modulus E is given in the material card rather than the shear modulus G. For instance Golding (2012) used Young's modulus. To see how the results are affected by that change, two analyses were run. In Figure 4.10 the results are presented. The shear modulus get a bigger mass failure than the elastic modulus, approximately at a penetration depth by 10 mm.

Which of the modulus there is preferred to use is difficult to determine. The elements start to fail approximately around a penetration

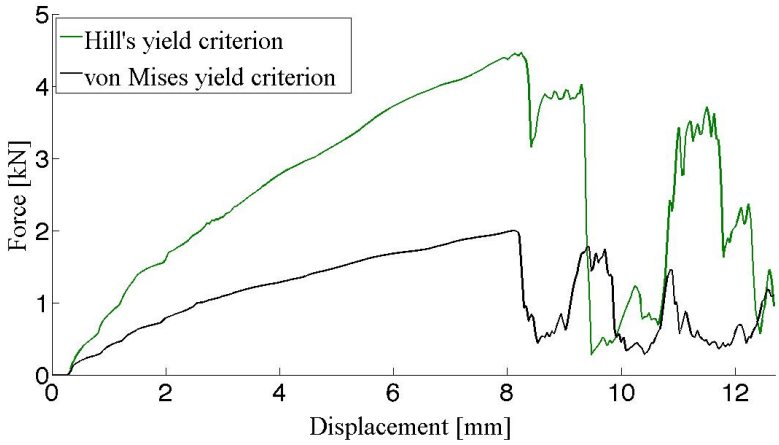

Figure 4.9: Hill's yield criterion compared with von Mises yield criterion. Shear modulus G and damage constant D1=0.04 are applied.

depth at 8mm for both cases, but the indenter in the analysis with the elastic modulus get faster contact with the ice. Which is seen from the curve, since the force increase more rapid after a drop.

To control the uniaxial stress for the analysis with Hill's criterion, D1=0.04 and shear modulus G, the values is calculated to 20 MPa. The penetration depth is 8.3mm at the peak force 4.4 kN.

In the case where the von Mises yield criterion is used, the uniaxial stress under the indenter is 9.7 MPa. The first drop is at 8.1 mm with a maximum force at 2 kN. Compared with the values from the section about compressive strength, the calculated values for uniaxial stress is sufficient.

4.2.4 Lemaitre Damage Model

The Lemaitre Damage model was one of the least demanding material models to run. There is an advantage that the damage constant is

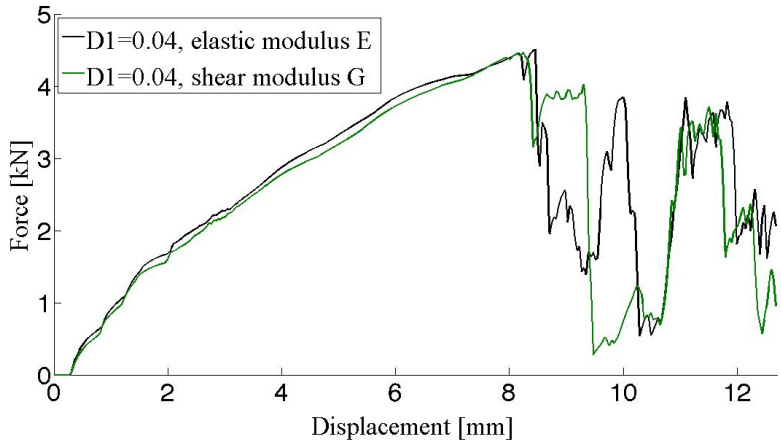

Figure 4.10: Comparison between Young's modulus E and shear modulus G with damage constant D1=0.04.

implemented. The parameters are tabulated in Table 3.5. Further three figures are presented to compare different values against each other.

Figure 4.11 gives a comparison between the smp and mpp version, described in Section 3.1. Two pair of similar input files have run differently. All four graphs give the saw tooth pattern, but mpp version do not have the big force drop. It is uncertain what happened with the two graphs with mpp version after 12.7 mm, but for the two other it seems to continue the brittle failure pattern. The smp version is further used, due to better results according to the calculated uniaxial stress described in the introduction.

In Figure 4.12 three graphs with different initial compressive stress σ_{y0} are compared, with equal damage constant and smp processing. The damage material constant S is renewed for each initial yield stress, $S = \sigma_{y0}/200$. The slope increase with higher value of the initial yield stress σ_{y0}. The Lemaitre Damage model depends to a certaint extent to these values.

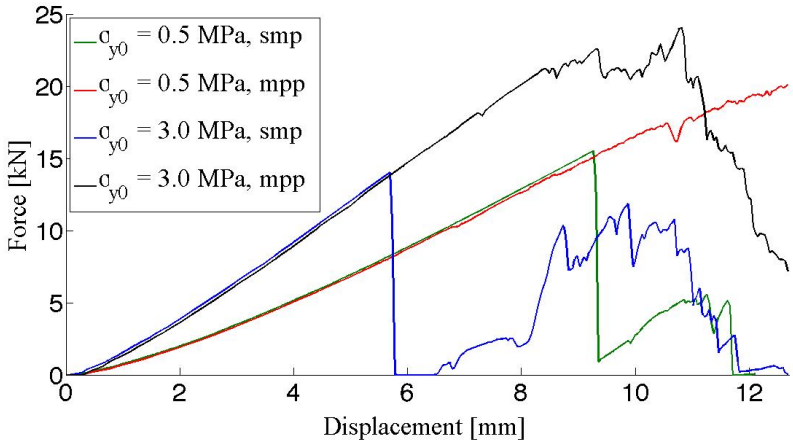

Figure 4.11: Comparison between smp and mpp with various initial compressive stress σ_{y0}.

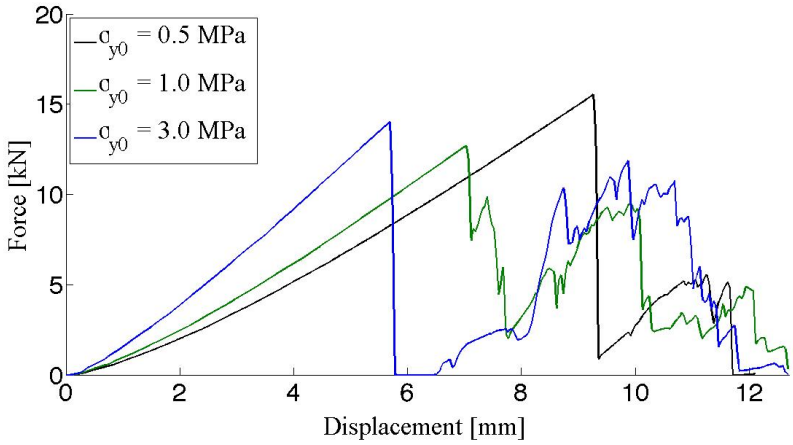

Figure 4.12: Lematire Damage model with various initial yield stress σ_{y0}. smp and Damage=0.350 are applied.

Figure 4.13 gives the results from three different damage constants, D_c. It is seen that the damage constant controls when the elements

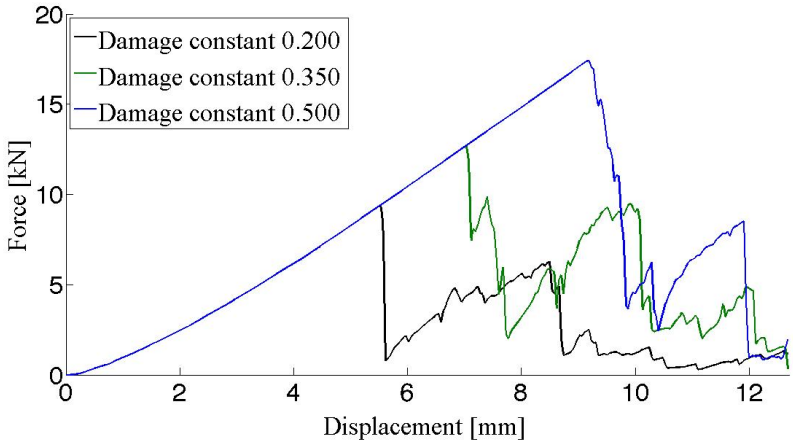

Figure 4.13: Lematire Damage model with various damage constant D_c, smp version.

goes to failure, higher damage constant gives a "delayed" deletion. The blue graph, D_c=0.500, is the default value in LS-Dyna. While, D_c=0.200 is the lowest recommended value according to Lemaitre and Desmorat (2010) and 0.350 is chosen as a average of those two. The damage constant at 0.350 gives an higher amplitude after failure compared to the others.

When D_c=0.200 the ice specimen starts to fail by the maximum force at 9.4 kN, by a penetration depth at 5.5 mm. D_c=0.350 and D_c=0.500 drop in force by 7 mm and 9.2 mm, respectively. The maximum force for the two latter are 12.2 kN and 17.4 kN.

By calculated uniaxial stress, given by the equation $F = \sigma/A$ the values for the last figure are higher than the given values in Section 2.2.1. The results for D_c=0.200, D_c=0.350 and D_c=0.500 are, respectively, 99 MPa, 79 MPa and 65 MPa.

Note that a comparison of the given results from the analyses with Lemaitre Damage model, the force-displacement history from von

Bock und Polach and Ehlers (2013) looks similar. In both cases the results are ductile and after a while drops the force.

4.2.5 Iso-Plot for First Principle Stress

An analysis from each material model are given in the iso-plots below. In the table caption the material model is given, while below which analysis is presented:

- Crushable Foam model; ν=0.003, $\sigma_t^c = 0.65$ MPa, σ_{max}=5 MPa
- Brittle Damage model; $G_c = 7.1\ J/m^3$, $\sigma_{max} = 8$ MPa
- Holmquist-Johnson-Cook model; D1=0.04, G=4.96 MPa
- Lemaitre Damage model: D_c=0.350, $\sigma_0 = 1$ MPa

The time history include six time steps, where the figures are named with related time step and displacement. The plots are half of the ice specimen, as shown in Figure 4.14. The fringe level range from 0 to 5 MPa, and apply to all iso-plots for easier comparison. The first principle stress is oriented in the vertical direction, parallell to the columns in the S2 sea ice.

As mentioned earlier, the shear band and extrusion of ice are not taken into account. The reason is the element erosion, i.e. the ice that should be extruded is deleted.

There is difference in how the indenter penetrates the ice specimen. For Crushable Foam no element erosion is developet, instead they expand out of plane where the indenter meets the ice. For Brittle Damage, Holmquist-Johnson-Cook and Lemaitre Damage model the element erosion occurs, and the elements starts to fail at different time steps.

The first failure that occurs with the Brittle Damage model, at a penetration depth at 2.7 mm, for HJC model by 8.3 mm and Lemaitre

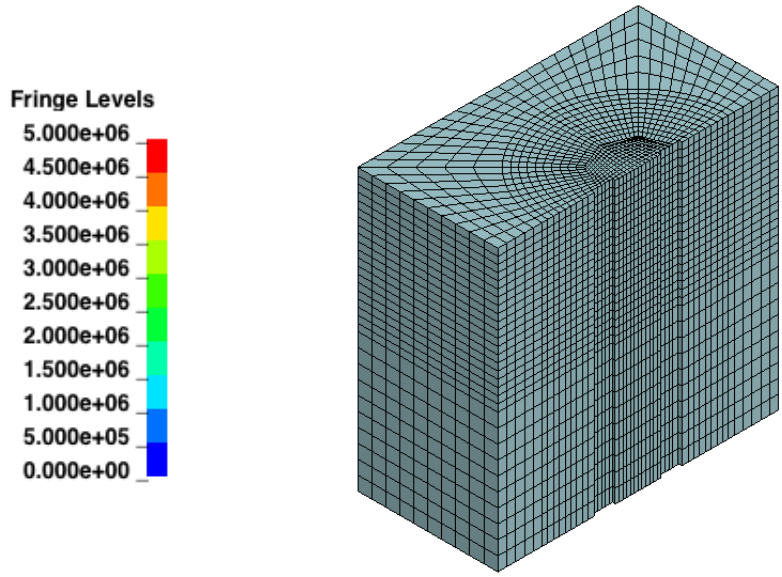

Figure 4.14: The fringe levels for first principal stress and half of the numerical ice specimen.

Damage model by 7.0 mm. The graphs are represented in Section 4.2, the figures 4.5, 4.10 and 4.12, respectively.

A criterion for brittle fracture is given for Crushable Foam and Brittle Damage model, the elements start to fail by the given maximum principal stress. The values are 5 MPa and 8 MPa, respectively. Failure occurs when the maximum principal stress reaches a critical value, $\sigma_1 \geq \sigma_{max}$.

In the ice specimen with the Lemaitre Damage model stress waves are develope before failure. After the first element failure, the high values of principle stress acts in the damage area.

Table 4.2: Iso-plot for the Crushable Foam model.

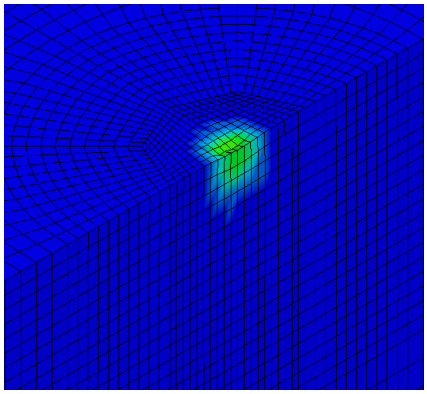

(a) t=0.4 s, 2.0 mm

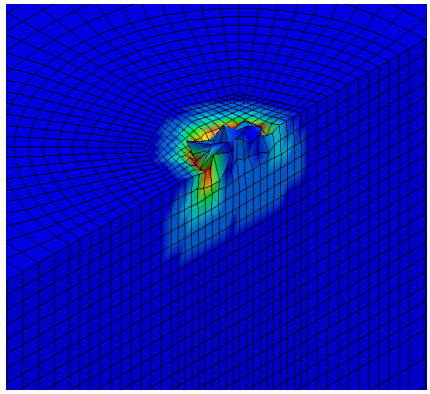

(b) t=1.36 s, 6.9 mm

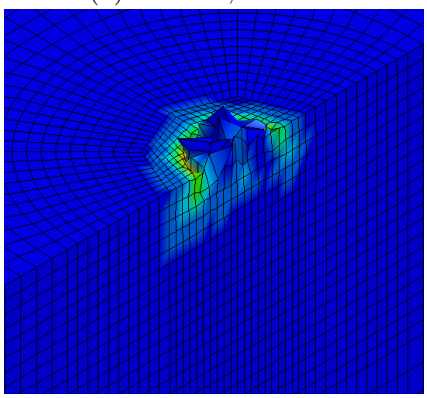

(c) t=1.68 s, 8.5 mm

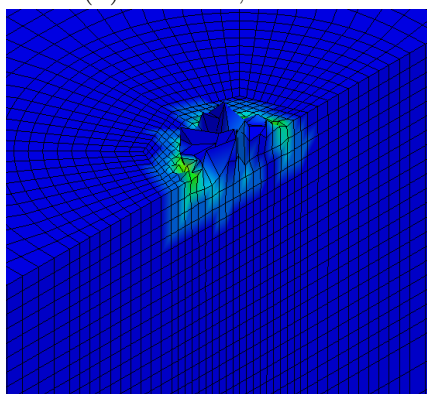

(d) t=2 s, 10.2 mm

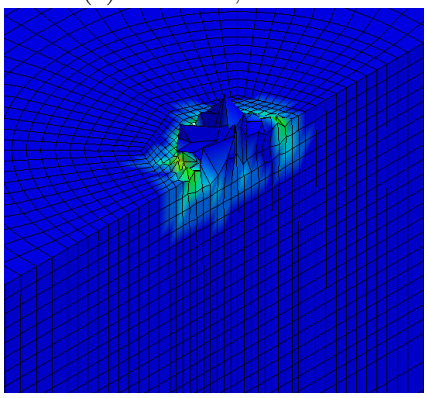

(e) t=2.24 s, 11.4 mm

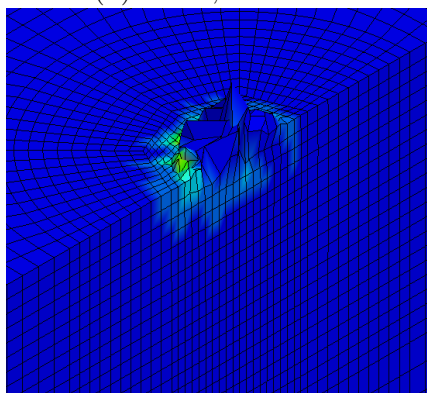

(f) t=2.5 s, 12.7 mm

Table 4.3: Iso-plot for the Brittle Damage model.

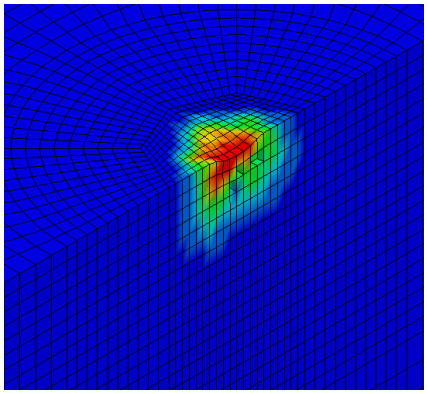

(a) t=0.4 s, 2.0 mm

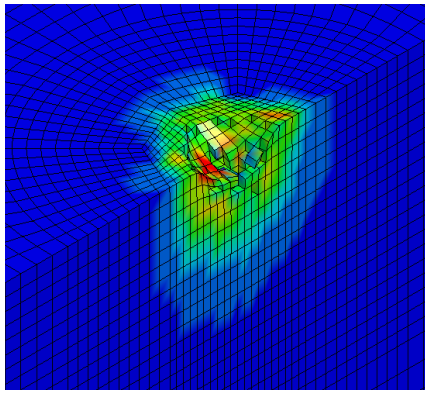

(b) t=1.36 s, 6.9 mm

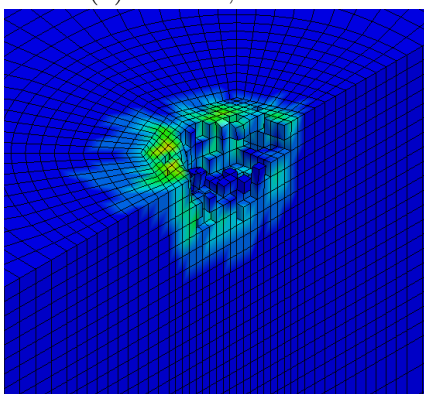

(c) t=1.68 s, 8.5 mm

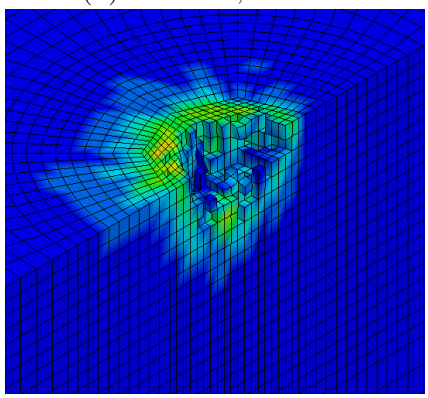

(d) t=2 s, 10.2 mm

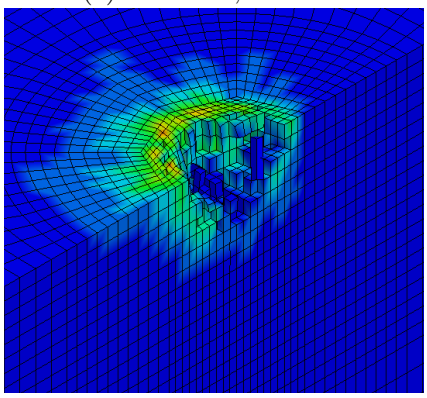

(e) t=2.24 s, 11.4 mm

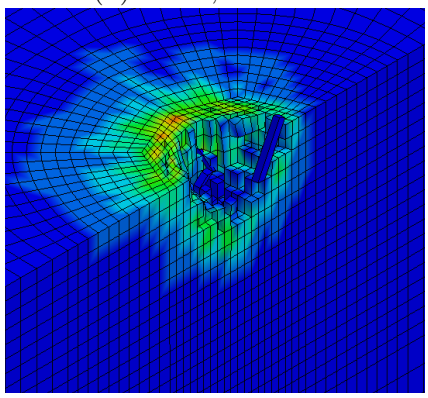

(f) t=2.5 s, 12.7 mm

Table 4.4: Iso-plot for the HJC model.

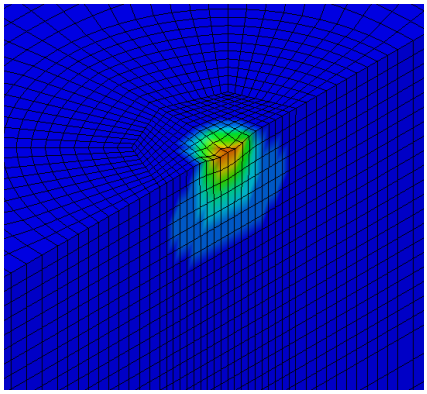

(a) t=0.4 s, 2.0 mm

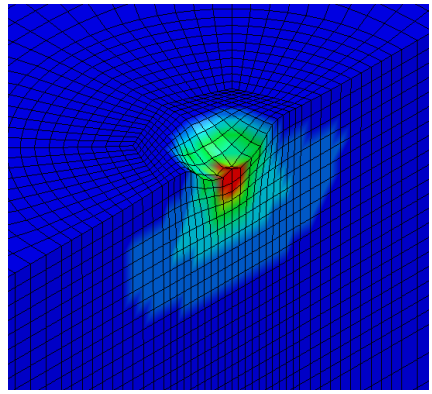

(b) t=1.36 s, 6.9 mm

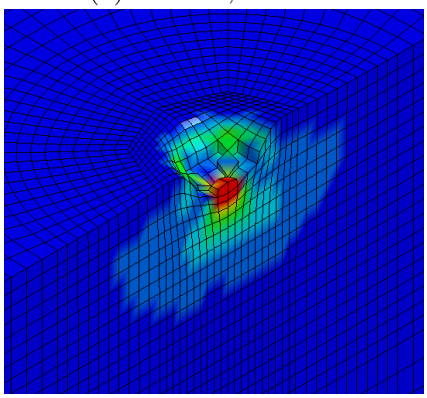

(c) t=1.68 s, 8.5 mm

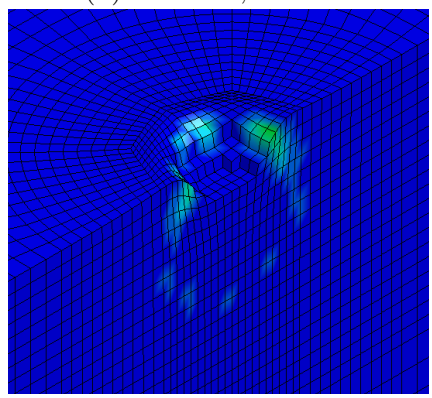

(d) t=2 s, 10.2 mm

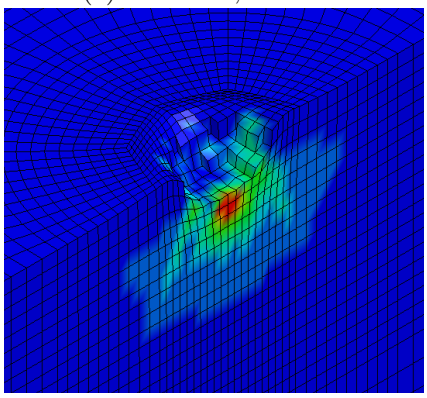

(e) t=2.24 s, 11.4 mm

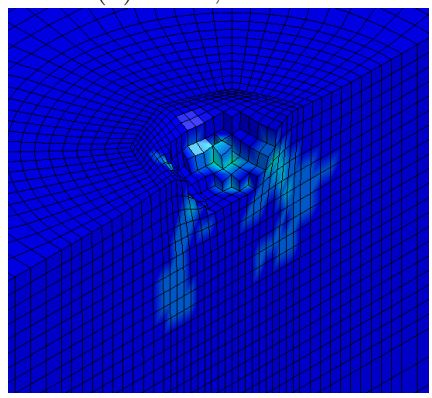

(f) t=2.5 s, 12.7 mm

Table 4.5: Iso-plot for the Lemaitre Damage model.

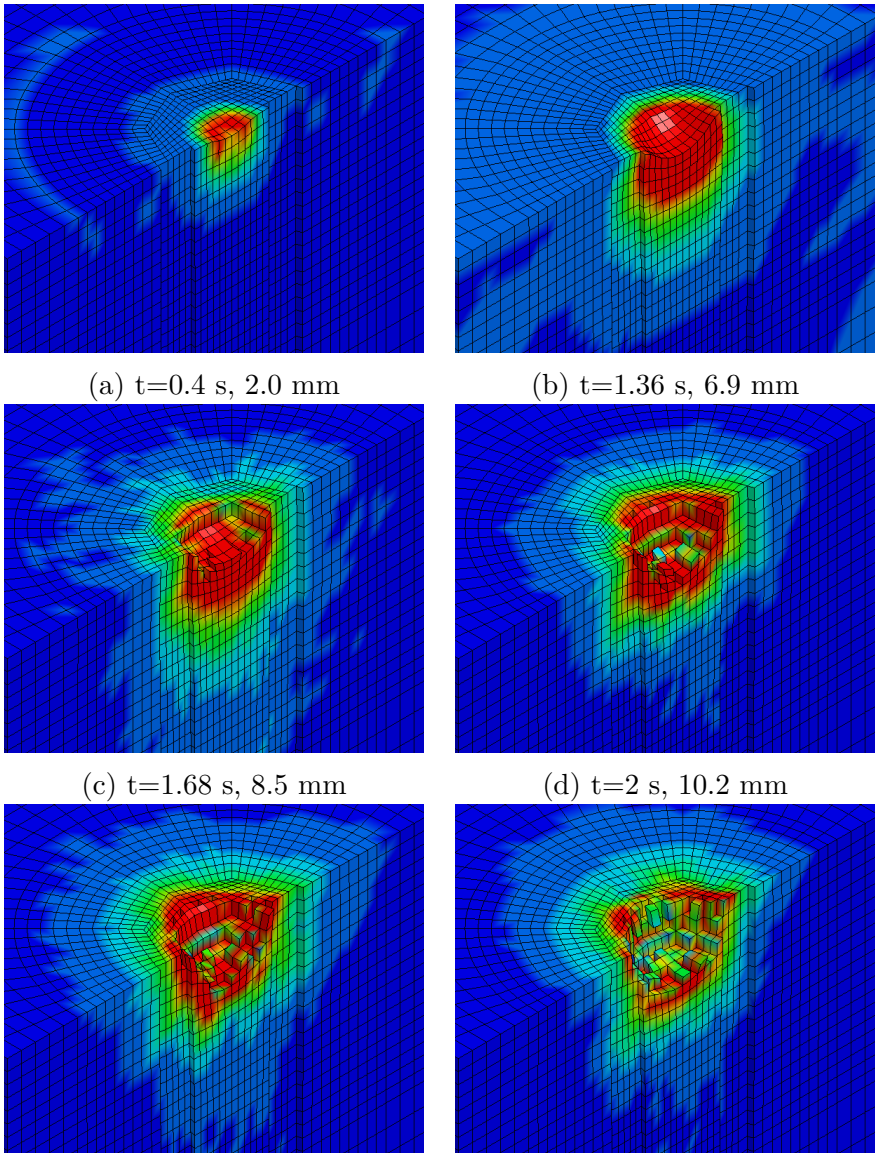

(a) t=0.4 s, 2.0 mm

(b) t=1.36 s, 6.9 mm

(c) t=1.68 s, 8.5 mm

(d) t=2 s, 10.2 mm

(e) t=2.24 s, 11.4 mm

(f) t=2.5 s, 12.7 mm

4.3 Results: Ice Sheet Towards an Offshore Structure

This numerical model is developed by Hilding et al. (2012), and is presented in Section 3.2.3. Further the results are presented for the drifting ice sheet towards an offshore structure.

In Figure 4.15 gives a graphical view of the analyses for the material models; the original model, Crushable Foam, Brittle Damage, HJC and Lemaitre Damage model. The comparison within the material models and the measurements from the the lighthouse Norströmsgrund in Figure 4.16 are further discussed in Chapter 5.

In the original paper the analyses were terminated after 20 seconds, here they are ended after 5 seconds due to little representative results.

Table 4.6: Ice actions from the analyses with an ice sheet towards an offshore structure

Material model	Force $[MN]$	time $[sec]$
Original model	1.81	2.1
Crushable Foam	2.80	2.3
Brittle Damage	4.63	1.1
HJC	3.33	5.0
Lemaitre Damage model	7.56	4.1

The maximum values are listed in Table 4.6. All results from the selected material models from LS-Dyna have higher values than the original material model. The Lemaitre Damage model gives the highest action, while the Crushable Foam model is closest to original model compared with the maximum values. For all material models the action from the interaction is in the right order of magnitude (MN). Compared with the average values from the lighthouse

Norströmsgrund at 2.1 MN to 3.5 MN, the Crushable Foam and HJC model give the nearest values.

In the original numerical simulation Young's modulus were determined to 5 GPa. First the analyses were run with 8 GPa, as for the numerical model with the ice specimen and the indenter. By a higher modulus the numerical model got unsatisfactory behaviour, so the modulus were assumed to 5 GPa. Those results have also some misbehaviors, given in Figure 4.15.

The figures in Table 4.7 view the different behaviour each analyses had at 5 seconds. The first figure view the original material model, where the ice being crushed in a controlled manner. The Crushable Foam and Lemaitre Damage model breaks the ice like a beam right in the front of the offshore structure. The Brittle Damage model causes that the element are blown up and fast erosion. The HJC model did not go to failure. That was also the case at a termination time at 10 seconds, the same compressive behaviour occured.

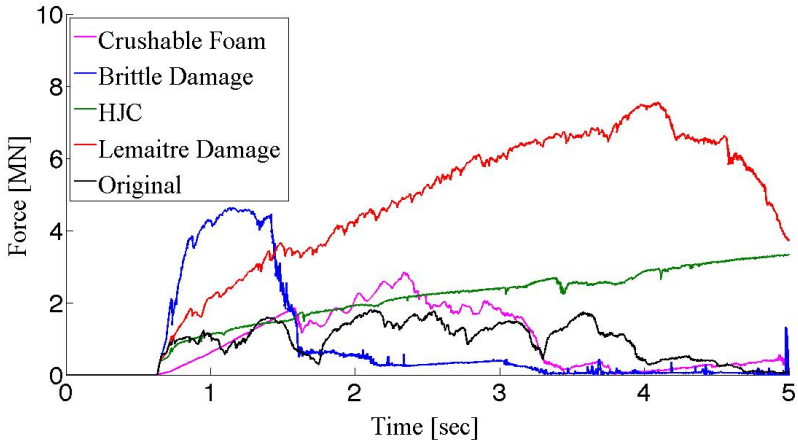

Figure 4.15: Comparison between the material models used in the numerical model of drifting ice sheet towards a structure.

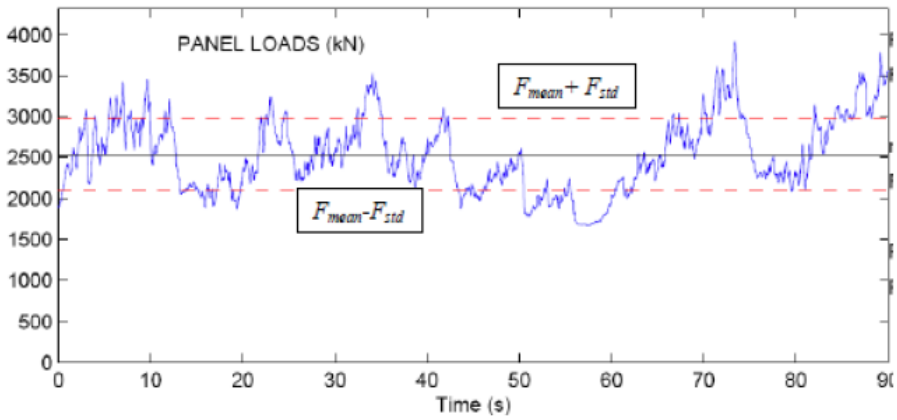

Figure 4.16: Measured total force applied on the lighthouse Norströmsgrund during a continuous crushing event. (Hilding et al., 2012)

Table 4.7: A plot for each material model at termination time, t=5sec, for the numerical model with the drifting ice sheet towards a structure

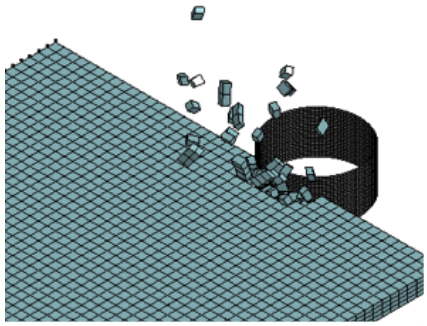

(a) Original

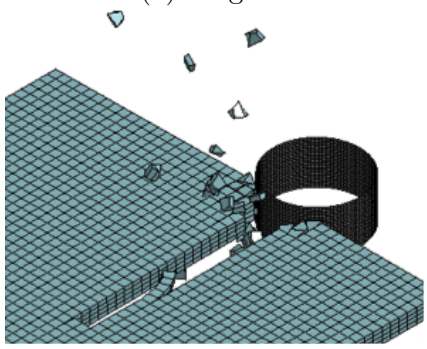

(b) Crushable Foam

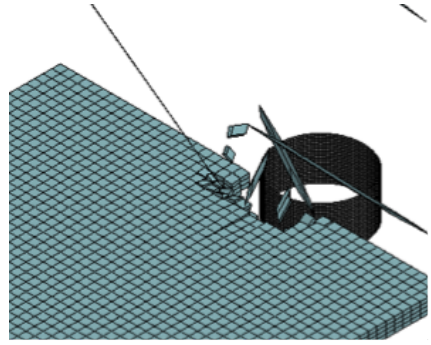

(c) Brittle Damage

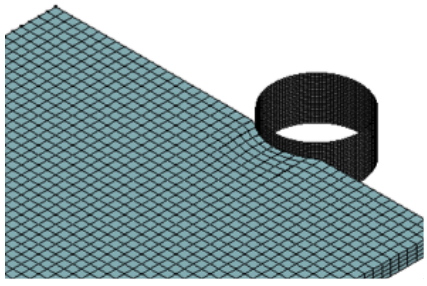

(d) HJC

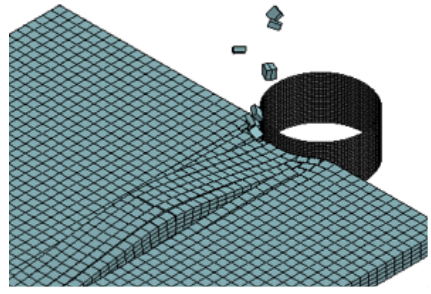

(e) Lemaitre Damage

Chapter 5

Discussion

In the introducing chapter, the main goal was introduced for this Master's thesis; to use existing material models from LS-Dyna to see if they can recreate the brittle failure for S2 sea ice under compression.

This chapter will discuss relevant results from each material model, and compared with each other. Further, some material models are compared with the measurements from the laboratory test by Kim et al. (2012). The numerical model developed by Hilding et al. (2012), will be discussed briefly at the end.

The brittle behaviour is described in Section 2.3, with a graphical view of an indentation test conducted by Kim et al. (2012). The same measurements are used in comparison with the discussed material models.

The force versus displacement curve for the material models, Crushable Foam, Brittle Damage, HJC and Lemaitre Damage model, have the desired sawtooth pattern and are in the right order of magnitude (kN). However, some models were better than others.

5.1 The Material Models

The material models were introduced in Section 2.7, characterised in Section 3.3 and the results from the analyses are presented in Chapter 4. They are further discussed individually, but mainly against each other.

A number of graphs have the characterised brittle failure in the force versus displacement figures. However, the desired behaviour was sought and found by inverse modelling. It was, for instance, easier to get a ductile behaviour than a brittle with the HJC model. Due to the sensitivity of the damage parameters.

The great advantage for the Crushable Foam, Brittle Damage and Lemaitre Damage model are the requirement of few parameters, while for HJC model has far more values to be characterised. There is although several aspects, i.a., CPU time, requirements according to the numerical input file and failure according to the elements.

In the litterature it is given the Brittle Damage model has its own damage rule, which depends on the shear retention and the shear strength. The model should also be suitable for compressive loading. Still, the indenter did not erode through the surface of the ice specimen. Therefore, the erosion criterion in LS-Dyna is used for the Brittle Damage model.

In the analyses with Crushable Foam, the results did not reflect the ice behaviour as good as desirable. Figure 4.3 view graphs that dampens out after maximum force, while Gagnon (2011) got sufficient results with the same model. A reason for the unfortunate results may be caused by disorderly indenter penetration, see the iso-plot in Table 4.2.

Numerical model

The difference between the numerical model with the confined ice specimen and the one Gagnon used with Crushable Foam model, is the shape of the ice specimen. His model is shaped like a pyramide and divided into several parts, where each part got their properties. The high and low stress curve were used in the same analysis, while in this context the curves are used separately.

It might be a problem that the ice specimen is confined when the Crushable Foam is applied, since the volume of compressed foams will naturally expand in any direction. Instead the elements expand out of the plane under the indenter. The problem may be solved if another numerical model is used, for instance an unconfined system or a full-scale model like the ice sheet towards an offshore structure.

The mesh density, of the numerical ice specimen from the indentation simulation, decrease from the inside out both horizontally and vertically. It was assumed that under the compressed area, the finite elements have approximately same size as the ice grains. Which means, there is not performed an optimalisation of the mesh.

From the iso-plots it seems that several elements fail at the same instance of time. Which causes a big drop in the force-displacment curve, and the values becomes close to zero after the maximum is reached. If an optimalisation of the mesh leads to increased density, the results for the Brittle Damage model may be more sufficient. The element erosion could potensially be more sufficient with a finer mesh, which may lead to better results.

An important aspect regarding the increased mesh density, is the duration of the analysis also increase. By explicit solution, the time step is limited by the element size and the speed of sound, $c = \sqrt{E/\rho}$, in the material. The smallest element in the mesh controls the time step for the whole solution.

As mentioned in the introduction to the result chapter, the CPU time was different for each material model. By an increased mesh density, HJC or Lemaitre Damage model would be preferred. If the iso-plots are studied for the those material models the element erosion by failure are sufficient.

The Force versus Displacement pattern

For the Crushable Foam the loading curve is essential as an input value, while the Brittle Damage mainly depends on the tensile cut-off of how the force-displacement curve develops. Failure in the HJC model is determined by plastic strain before fracture ε_{min}, the damage constant $D1$ and the erosion criterion FS (failure strain) by calculation and inverse modelling. While, failure by the Lemaitre Damage model are determined more easily with the damage constant D_c.

From the results in Chapter 4 it seems to be the material models that include a damage constant that gives the best results. The figures 4.10 and 4.13 view the final force pattern to HJC and Lemaitre Damage model, respectively. Although the inception gives a ductile behaviour, the first force drop develops when the first element goes to failure. It would be preferred if the elements failed earlier, since the penetration depth was at 12.7 mm and the termination time at 2.5 seconds.

How will the load pattern evolve if the termination time were 5 seconds instead of the current 2.5 seconds? The corresponding graph to Crushable Foam and Brittle Damage might view another loading path, where the force increased due to more compressed material or better contact between the indenter and the ice specimen.

If the simulation continued, hopefully, the loading pattern for HJC and Lemaitre Damage model still had the sawtooth pattern and gave sufficient results.

von Mises and Hill's yield criterion

The results from HJC is interesting regarding the isotropic and anisotropic effect. Figure 4.9 compare the results from von Mises and Hill's yield criterion, i.e., isotropic and anisotropic consideration. Suprisingly the action from the transversly isotropic sea ice is approxiamately 100 % higher than for isotropic sea ice. If the actions are higher with an anisotropic consideration, they can not be neglected.

It is an interesting discovery, since it can be essential to which material models one chose in further studies. There are several material models implemented in LS-Dyna that takes the anisotropic effect into account. Note that those models can require parameters which is unknown for ice.

5.2 Comparison with Laboratory Tests

Interaction Between Ice Specimen and Indenter

Brittle Damage, HJC and Lemaitre Damage model are taken into further discussion, where the simulation results are compared with the laboratory test by Kim et al. (2012). Of clearity, it is the same experiment as the main numerical model with the indenter and the confined ice specimen. The Crushable Foam model is disregarded due to the results presented in Chapter 4. The elements under the indenter blowed up and the force dampens out in the force-displacement history, hence the results may be uncertain.

The comparison between the numerical simulation and laboratory tests are not optimal, since the laboratory tests are with freshwater ice. Sea ice is weaker than freshwater ice, which cause a lower loading pattern for the curves. Anyway, all other conditions are equal. The comparison is viewed in the figures 5.1a and 5.1b.

Test number EK7 and EK8 show brittle fracture, and the ice fails without previous plastic deformation. The three numerical results have a ductile behaviour before fracture. It is the Lemaitre Damage model that gives the best results. The material model shows good correspondency with the test in Figure 5.1a.

Ice Sheet Towards a Offshore Structure

By a comparison between the numerical results and the lighthouse, Figure 4.15 against Figure 4.16, it is seen that the numerical simulations is in right order of magnitude (MN) compared to the average force level from the lighthouse.

For the numerical model, there is room for improvement. In this thesis, the cohesive elements were included. Although the failure criterion for the cohesive elements were set above the continuum elements, it is likely that they will affect the results.

The failure at the termination time is viewed in Table 4.7, for each material model. The behaviour is quite different compared to the original model. The Crushable Foam and Lemaitre Damage model compress the ice like a beam, and the ice fails unlikely. While, the Brittle Damage erode the elements fast, so the contact between the ice sheet and the offshore structure is lost. The ice sheet being compressed without failure in the case with HJC model.

The change in Young's modulus, from 8 GPa to 5 GPa was more important than first expected. There is known that the modulus for sea ice is lower than for freshwater ice, and the value of 8 GPa can also be used to freshwater ice. Since the modulus was important to the development of interaction, the modulus might have to be lower than 8 GPa.

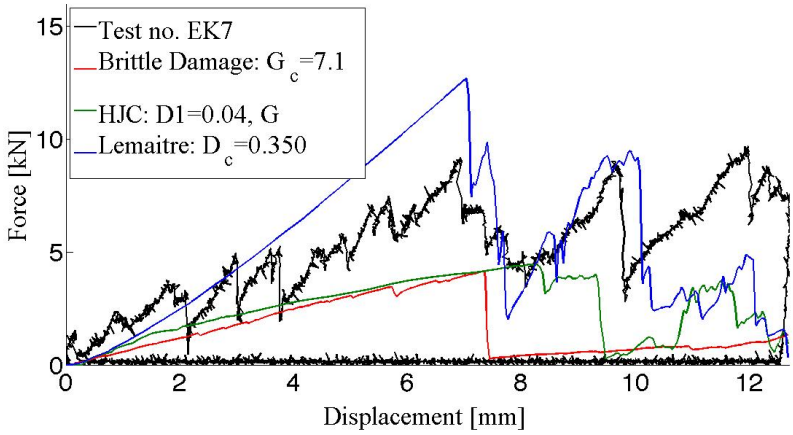

(a) Test no. EK7

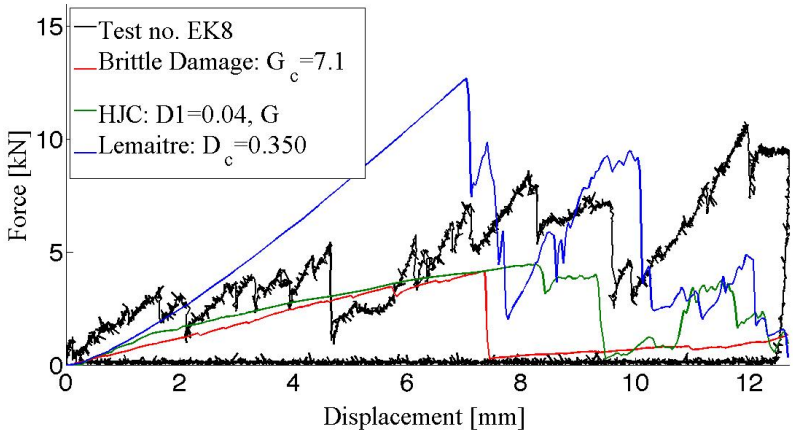

(b) Test no. EK8

Figure 5.1: Comparison between Brittle Damage, HJC, Lemaitre Damage model and experimental measurements test no. (a) EK7 and (b) EK8

Chapter 6

Conclusion

The main purpose in this thesis was to see if already implemented material models in LS-Dyna could recreate brittle failure of S2 sea ice under interaction with an offshore structure. Three numerical models were used; a single volume element, interaction between a confined ice specimen and an indenter, and a drifting ice sheet towards an offshore structure.

Four different material models were characterised and used in the numerical simulations. The chosen were Crushable Foam, Brittle Damage, Holmquist-Johnson-Cook (HJC) and Lemaitre Damage model.

The main part of the results consisted of the model based on the laboratory test conducted by Kim et al. (2012). The numerical model was an indenter penetrating a confined ice specimen, i.e. a triaxial loading which compliance the behaviour of an ice floe.

The force versus displacement history from the numerical simulation were compared with small and large scale tests.The material models gave the desired sawtooth pattern and results in the right order of magnitude. However, some results were more sufficient than others.

Material models with an already implemented damage constant, i.e.

HJC and Lemaitre Damage model, are simpler to determine the desired behaviour due to inverse modelling of the damage constant. Even though the HJC model has several material parameters that should be determined, it gives the desired brittle failure in the loading curve.

If numerical simulations can replace some of the experimental tests, the design of offshore structure against ice actions can be more cost efficient and less time consuming.

By improvement, it seems possible to find an existing material model that can give sufficient results regarding the desired brittle failure by an ice-structure interaction. Further research is required, and in next chapter there are some suggestions.

Chapter 7

Further Work

Suggestions according to improvement and further research are listed below:

- The numerical model itself can be improved, e.g. another structure, an optimalisation of the mesh and liquid layer on top as von Bock und Polach and Ehlers (2013). There is also of interest to take the friction into consideration.
- In order to find a material model that corresponds to the brittle behavior to ice, it may be advantageous to perform tests on ice for further use in a numerical simulation. And at the end compare the measurements from laboratory with those from the analyses.
- Use of the Smooth Particle Hydrodynamics (SPH) in LS-Dyna can be an efficient tool for penetration. It is a meshfree method that can simulate solids and solve problem where finite element method has difficulties.
- In this thesis the HJC material model was also implemented in IMPETUS Afea Solver, a software for linear and non-linear computational mechanics. The result was not sufficient at the

first try, but with some more time according to the numerical model set-up the results may be sufficient.

- There is also necessary to see if other material models can be used instead of those who are presented in this Master's thesis, e.g. anisotropic material models.

Bibliography

Børvik, T. and Hopperstad, O.S. Compendium in tkt 4135 mechanics of materials. *Norwegian University of Science and Technology, Trondheim*, 2013.

Dempsey, J.P.; Adamson, R.M., and Mulmule, S.V. Scale effects on the in-situ tensile strength and fracture of ice. part II: First-year sea ice at resolute, nwt. *International journal of fracture*, 1999.

Dykins, J.E. Ice engineering-tensile properties of sea ice grown in a confined system. *DTIC Document*, 1970.

Gagnon, R.E. A numerical model of ice crushing using a foam analogue. *Cold Regions Science and Technology*, 2011.

Gagnon, R.E. and Derradji-Aouat, A. First results of numerical simulations of bergy bit collisions with the CCGS Terry Fox Icebreaker. *IAHR*, 2006.

Gagnon, R.E. and Wang, J. Numerical simulations of a tanker collision with a bergy bit incorporating hydrodynamics, a validated ice model and damage to the vessel. *Cold Regions Science and Technology*, 2012.

Gammon, P.H.; Kiefte, H., and Clouter, M.J. Elastic constants of ice samples by brillouin spectroscopy. *The Journal of Physical Chemistry*, 1983.

Golding, N. Compressive shear faulting in ice loaded triaxially: The influence of confinement. *Doctoral Thesis, Dartmouth College*, 2012.

Govindjee, S.; Kay, G.J., and Simo, J.C. Anisotropic modelling and numerical simulation of brittle damage in concrete. *International Journal for Numerical Methods in Engineering*, 1995.

Gratz, E.T. and Schulson, E.M. Brittle failure of columnar saline ice under triaxial compression. *Journal of Geophysical Research: Solid Earth (1978–2012)*, 1997.

Hallquist, J.O. LS-Dyna 3D keyword user's manual. *Livermore Software Technology Corporation*, 1998.

Hallquist, J.O. LS-Dyna 3D keyword user's manual. *Livermore Software Technology Corporation*, 2014.

Hilding, D.; Forsberg, J., and A., Gürtner. Simulation of loads from drifting ice sheets on offshore structure. *12th LS-Dyna User Conference*, 2012.

Holmquist, T.J.; Johnson, G.R., and Cook, W.H. A computational constitutive model for concrete subjected to large strains, high strain rate, and high pressures. *14th international symposium on ballistics*, 1993.

Iliescu, D. and Schulson, E.M. Brittle compressive failure of ice: monotonic versus cyclic loading. *Acta materialia*, 2002.

Johnson, G.R.; Beissel, S.R.; Holmquist, T.J., and Frew, D.J. Computed radial stresses in a concrete target penetrated by a steel projectile. *Proceedings of the 5th International Conference on Structures under shock and impact, Portsmouth, UK*, 1998.

Jones, S.J. High strain-rate compression tests on ice. *The Journal of Physical Chemistry B*, 1997.

Kim, E.; Golding, N.; Schulson, E.M.; Løset, S., and Renshaw, C.E. Mechanisms governing failure of ice beneath a spherically-shaped indenter. *Cold Regions Science and Technology*, 2012.

Kolari, K. Damage mechanics model for brittle failure of transversely isotropic solids: Finite element implementation. *VTT Technical Research Centre of Finland*, 2007.

Lemaitre, J. and Desmorat, R. Engineering damage mechanics: ductile, creep, fatigue and brittle failures. *Springer*, 2010.

Leppänen, J. Dynamic behaviour of concrete structures subjected to blast and fragment impacts. *Chalmers University of Technology*, 2002.

Løset, S.; Shkhinek, K.N., and Høyland, K.V. Ice physics and mechanics. *Norwegian University of Science and Technology, Trondheim*, 1998.

Løset, S.; Shkhinek, K.N.; Gudmestad, O.T., and Høyland, K.V. Actions from ice on arctic offshore and coastal structures. *LAN, Trondheim, St. Petersburg, Moscow, Krasnodar*, 2006.

Michel, B. and Ramseier, R.O. Classification of river and lake ice. *Canadian Geotechnical Journal*, 1969.

Richter-Menge, J.A. and Jones, K.F. The tensile strength of first-year sea ice. *U.S. Army Cold Regions Research and Engineering Laboratory, Hanover, New Hampshire, USA*, 1993.

Saeki, H. and Ozaki, A. Physics and mechanics of ice. *Springer*, 1980.

Saeki, H.; Nomura, T., and Ozaki, A. Experimental study on the testing methods of strength and mechanical properties for sea ice. *Proc. IAHR Symposium on Ice Problems, Lulea, Sweden*, 1978.

Schulson, E.M. Brittle failure of ice. *Engineering Fracture Mechanics*, 2001.

Schulson, E.M. Columnar ice sections, figures, 2010.

Schulson, E.M. personal communication, 08-04-2014, 2014.

Schulson, E.M. and Duval, P. Creep and fracture of ice. *Cambridge University Press Cambridge*, 2009.

Schulson, E.M. and Gratz, E.T. The brittle compressive failure of orthotropic ice under triaxial loading. *Acta materialia*, 1999.

Seah, C.C. Penetration and perforation of granite targets by hard projectiles. *Doctoral Thesis, Norwegian University of Science and Technology*, 2006.

Sodhi, D.S. and Haehnel, R.B. Crushing ice forces on structures. *Journal of cold regions engineering*, 2003.

Timco, G.W. and Weeks, W.F. A review of the engineering properties of sea ice. *Cold Regions Science and Technology*, 2010.

von Bock und Polach, R. and Ehlers, S. Model scale ice – part B: Numerical model. *Cold Regions Science and Technology*, 2013.

Weeks, W.F. and Assur, A. The mechanical properties of sea ice. *DTIC Document*, 1967.